Chapter 6

Two-dimensional Faceting

From the previous investigations in this work it is known that there is enhanced interfacial stability between ionic insulators and stepped metal surfaces in the case of suitable geometrical matching between the charge modulation of the substrate and the ions in the adlayer. Corresponding cases leading to epitaxial layer growth have been discussed in chapter 4. This stability can be also exploited to fabricate one-dimensional "hill-and-valley" facet structures (e.g. KCl/Ag(211), chapter 5) if the actual crystallographic orientation of the template is close to a substrate orientation, where enhanced interfacial stability between adlayer and substrate occurs. Consequently, it should be possible to expand this principle to a two-dimensional faceting of kinked substrates. In this chapter I will show the results of the investigation of such a system, **NaCl on Cu(532)**, which was used to fabricate highly regular pyramidal facet structures.

The (532) surface has features of the (211) surface – namely (111) microfacets separated by intrinsic (100) steps – and additionally consists of regular kinks incorporated into the close-packed Cu rows located at the step edges (cf. Figure 3.3). These features condition the starting surface in a way so that the fabrication of a quasi-two-dimensional facet array (i.e. a pyramidal structure) should be possible with this Cu(532) surface.

After demonstrating the fabrication of a two-dimensional facet array, this prestructured surface will be used to verify the chemical selectivity of the template by adsorbing CO and depositing Ag, respectively.

6.1 NaCl on Cu(532)

This system was investigated using the complementary methods of electron diffraction and scanning tunneling microscopy. The results obtained from both methods will be compared and combined. The STM images and the respective hard-sphere models will be oriented in the same

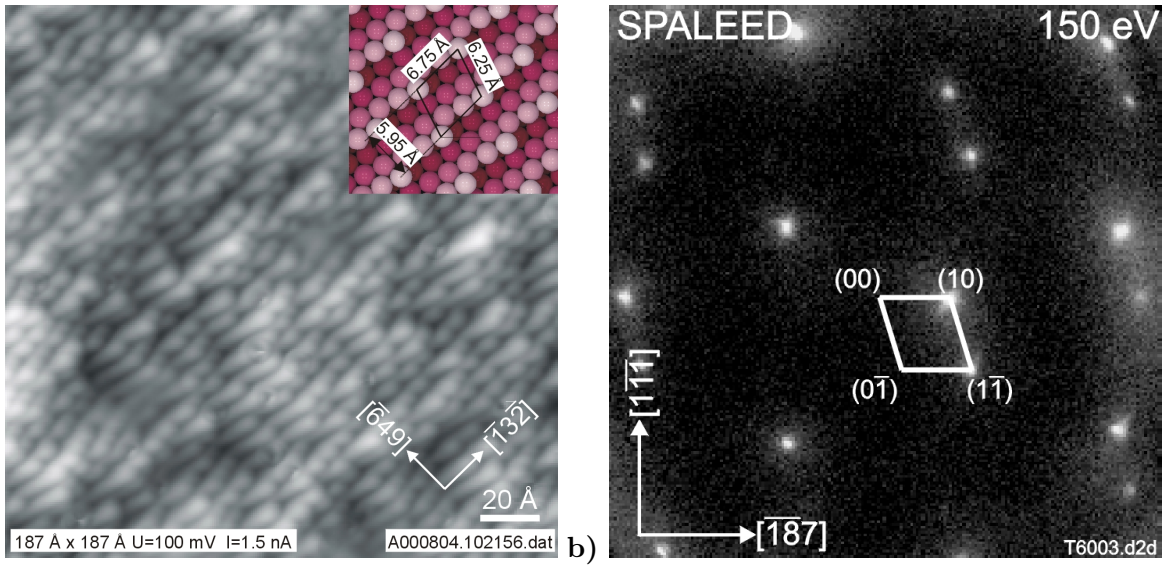

Figure 6.1: STM image and diffraction pattern of the clean Cu(532) surface
a) STM image (187 Å × 187 Å, U=100 mV, I=1.5 nA) with the inset showing a hard-sphere model of the (532) surface in the same azimuthal orientation
b) diffraction pattern taken at 150 eV with reciprocal Cu(532) surface unit cell; only a few spots of the diffraction pattern are seen at this energy due to strong Bragg modulation of the spot intensity of this surface

azimuthal angle for an easier comparison between both.

6.1.1 Cu(532) Surface

The Cu(532) sample was prepared according to the method described in section 1.3. The STM image taken after several sputtering and annealing cycles can be seen in Figure 6.1a. Extended terraces corresponding to the bulk-terminated (532) structure could not be observed, although different annealing and cooling procedures were applied during the sample preparation of the Cu(532) substrate. In a two-dimensional Fourier transformation of the STM image, discrete satellites in the $[\bar{6}49]$ direction, i.e. perpendicular to the intrinsic (100) steps were observed. This indicates a long-range correlation along this direction. The corresponding average distance determined from this two-dimensional Fourier transformation is given by about 5.9 Å. This is close to the theoretical value of 5.95 Å for the separation of kink rows running along $[\bar{1}3\bar{2}]$. Along these kink rows, however, no long-range ordering was found. The kink spacing along this direction is not well defined on a global scale. Nevertheless, locally bulk-terminated areas can be observed in the STM image. The root mean square deviation of the height distribution in the STM image was determined to about 0.75 Å. This indicates that no tremendous vertical

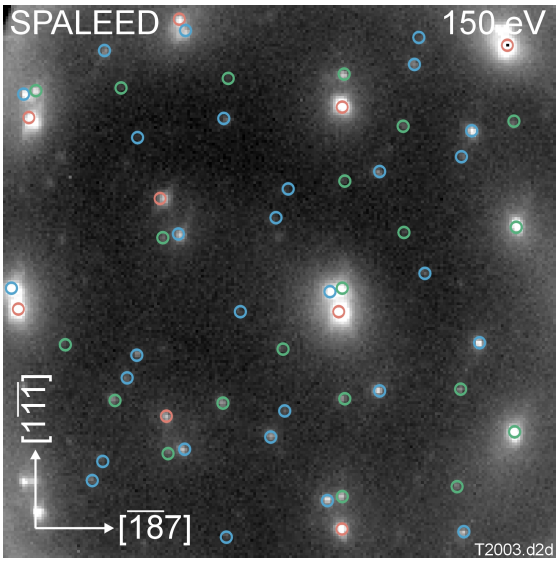

Figure 6.2: Diffraction pattern of the faceted Cu(532) surface after the deposition of 0.6 ML NaCl at 600 K
spots are color-coded according to the facets they belong to: Red = (111), green = (311), and blue = (531); all spots are changing their position with respect to $k_{\parallel}$ while changing the electron energy which indicates a faceting of the surface

roughness at a mesoscopic scale can be found and the surface can be used for the deposition experiments.

A diffraction pattern of the Cu(532) surface at an electron energy of 150 eV is shown in Figure 6.1b. Compared with the diffraction pattern calculated for this surface (Figure A.3), just a few spots are visible at this energy. Due to the small interlayer spacing of d=0.29 Å the in-phase scattering conditions for a given lattice rod (the latter are equivalent to the condition that $k_{\perp} = n\frac{2\pi}{d}$, with n an integer) are far apart in k-space. Therefore, only a few spots are visible at a particular energy. A systematic measurement of the diffraction patterns taken at a wide range of energies (80 eV to 270 eV) and a comparison with the energies calculated for Bragg reflections (hkl) show that the scattered intensity is indeed confined to the vicinity of the Bragg points. With these results it is possible to identify particular lattice rods and to plot the surface unit cell into Figure 6.1b.

6.1.2 NaCl Deposition

From previous experiments with Cu(211) as a template for the alkali halide deposition [FHZ$^+$00, FHR$^+$02] it is known that at temperatures above 300 K the copper atoms are mobile enough to form adsorbate-induced facets. For the system NaCl/Cu(532), a faceting process occurs at

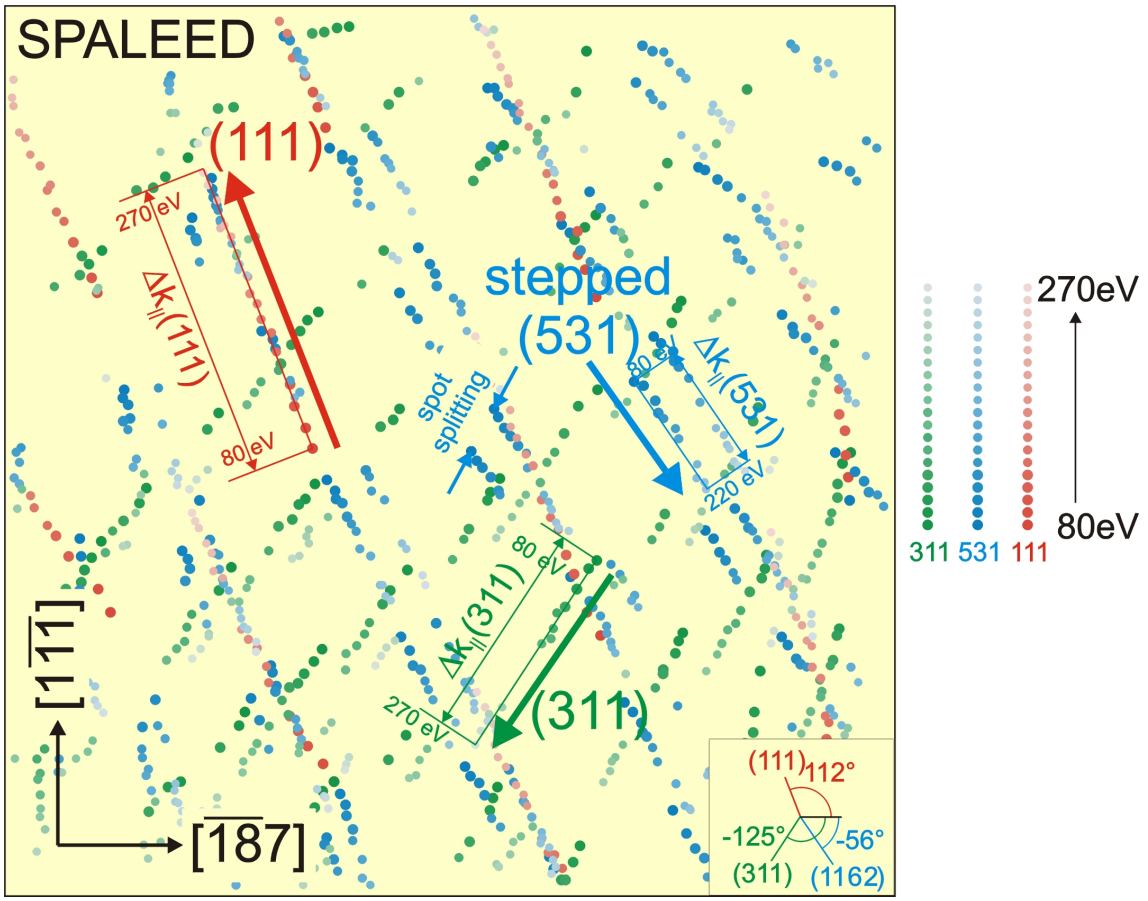

Figure 6.3: Analysis of the facet orientations using a set of diffraction patterns
This scheme is produced by the following procedure: A sequence of diffraction patterns was taken at energies between 80 eV and 270 eV with the wave vector component $k_\perp$ normal to the (532) surface. The spot positions obtained from the set of diffraction patterns are summarized in this scheme, which is a projection of the facet rods into the paper plane. The color and tinge of the spots represent the respective facets and energies: Red spots belong to the (111) facet, green to the (311) facet, and blue to the stepped (531) facet. In the lower right corner the azimuthal angles of the facets are indicated when projecting the facet rods into the paper plane. The horizontal $[\overline{1}87]$ direction defines an angle of 0°.

substrate temperatures between 500 K and 600 K. Below these temperatures no faceting effect was observed. The reason for this different temperature behavior can be attributed to the circumstance, that a higher mass transport is necessary to achieve the pyramidal structure described in the following, and that the mass transport on a stepped surface is more effective than on a kinked surface [Sto94].

One part of the experiments with this system was carried out using the SPA-LEED instrument. The diffraction patterns will be used to determine the orientation of the facets. In comparison to the clean surface, the diffraction patterns obtained after depositing about 0.6 monolayers NaCl onto the Cu(532) surface at 600 K (cf. Figure 6.2) consist of three sets of spots which change their position with respect to $k_{\parallel}$ while changing the electron energy. Consequently, the spots are located on facet rods which are, in contrast to the (532) lattice rods, inclined with respect to the normal of the macroscopic surface. The spots belonging to a particular facet type could be identified and were color-coded in Figure 6.2. The positions of the three sets of spots change with increasing electron energy in three diagonal directions: The red set from down right to up left, the green set from up right to down left, and the blue set from up left to down right. The previously used gray-scale plots of the LEED intensity $I(k_{\perp},k_{\parallel})$ do not serve as an adequate evaluation procedure for the complex facet structure observed here. Alternatively, the orientations of the tilted facet rods can be calculated in the following: A sequence of diffraction patterns taken at energies between 80 eV and 270 eV with the wave vector component $k_{\perp}$ normal to the (532) surface was recorded without any readjustment of the sample position or other parameters. Afterwards, a set of diffraction patterns of the clean surface was recorded at identical measurement parameters. Comparison of these two sets of diffraction patterns allowed to compensate for potential energy-dependent drifts in the spot position. The spot positions obtained from the corrected set of diffraction patterns which are representative for the facet structure are summarized and illustrated in Figure 6.3. The color of the spots corresponds to the respective facet, and the tinge is correlated with the electron energy, which can be seen in the scale on the right hand side. The obtained scheme thus shows the projection of the different facet rods into the paper plane. With this information, one can calculate the inclination of the facet rods from the change in the lateral position $\Delta k_{\parallel}$ and the change in the vertical position $\Delta k_{\perp}$ (electron energy) in the three-dimensional reciprocal space. The azimuthal angle of the projected facet rods is indicated in the right bottom corner of Figure 6.3 with the horizontal $[\overline{1}87]$ direction defining an angle of 0°. The orientations clearly determined are the **(111)** (red circles) and the **(311)** (green circles) orientation. The orientation of the third facet is more complicated: It can be described as a stepped **(531)** facet, whose step characteristics is apparent from the spot splitting seen in Figure 6.3 (cf. indication by arrows in the center of the figure). The stepped structure of the (531) facet, which will be discussed later in greater detail, results

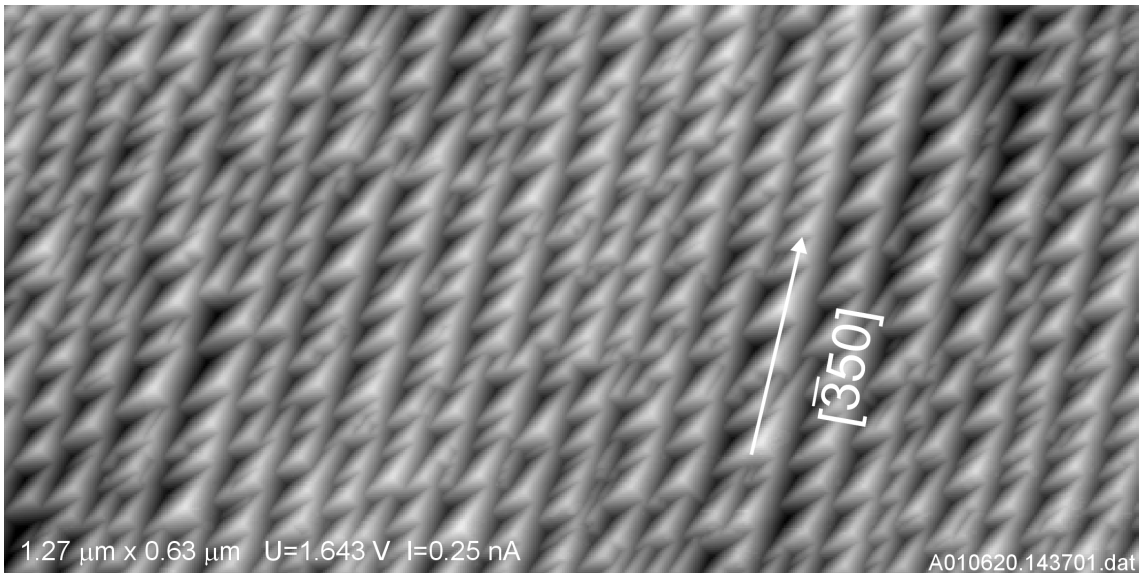

Figure 6.4: Overview STM image (1.27 μm × 0.63 μm, U=1.643 V, I=0.25 nA) of the facet structure after the deposition of 0.6 ML NaCl onto the Cu(532) surface at 600 K; staircase-like columns are aligned with the [$\bar{3}$50] direction which are separated by extended facets

in a (11 6 2) orientation. The polar angle between the (532) surface and the identified facets is 20.5° for the (111) facet, 12.0° for the (311) facet, and 10.1° for the (11 6 2) facet.

The structure of this faceted surface will now be investigated by STM. A necessity for imaging a surface with a large height modulation is to avoid so-called double (or even multiple) STM tips. If such a surface is imaged with a double tip, additional features appear in the image, and the real structure is falsified. The result of 0.6 ML NaCl deposition onto the Cu(532) surface at 600 K can be seen in the STM image in Figure 6.4 (size 1.27 μm × 0.63 μm). The former flat surface is completely reorganized into a regular structure of three-sided pyramids. Two of the three facet types form staircase-like columns, which are aligned with the [$\bar{3}$50] direction and separated by extended facets of the third type. A closer look at this structure is shown in the STM images in Figures 6.5a and 6.6, where areas of 3150 Å × 3150 Å and 70 Å × 80 Å, respectively, are mapped. From the SPA-LEED information concerning the facet orientations, the facets in the STM images can be assigned accordingly (Figure 6.5a). The gray scale plot in Figure 6.5b shows the self-correlation function of the STM image in Figure 6.5a. The self-correlation function is defined as: G(k1,k2)=$\sum$f(x,y)·f(x+k1,y+k2), where f(x,y) is the image matrix. The calculation of the self-correlation is equivalent to the superposition of the original image and the same image shifted by a vector (k1,k2) with respect to the center of the image. The resulting image, G(k1,k2), is a measure of how different the two images are. The more similar the original image

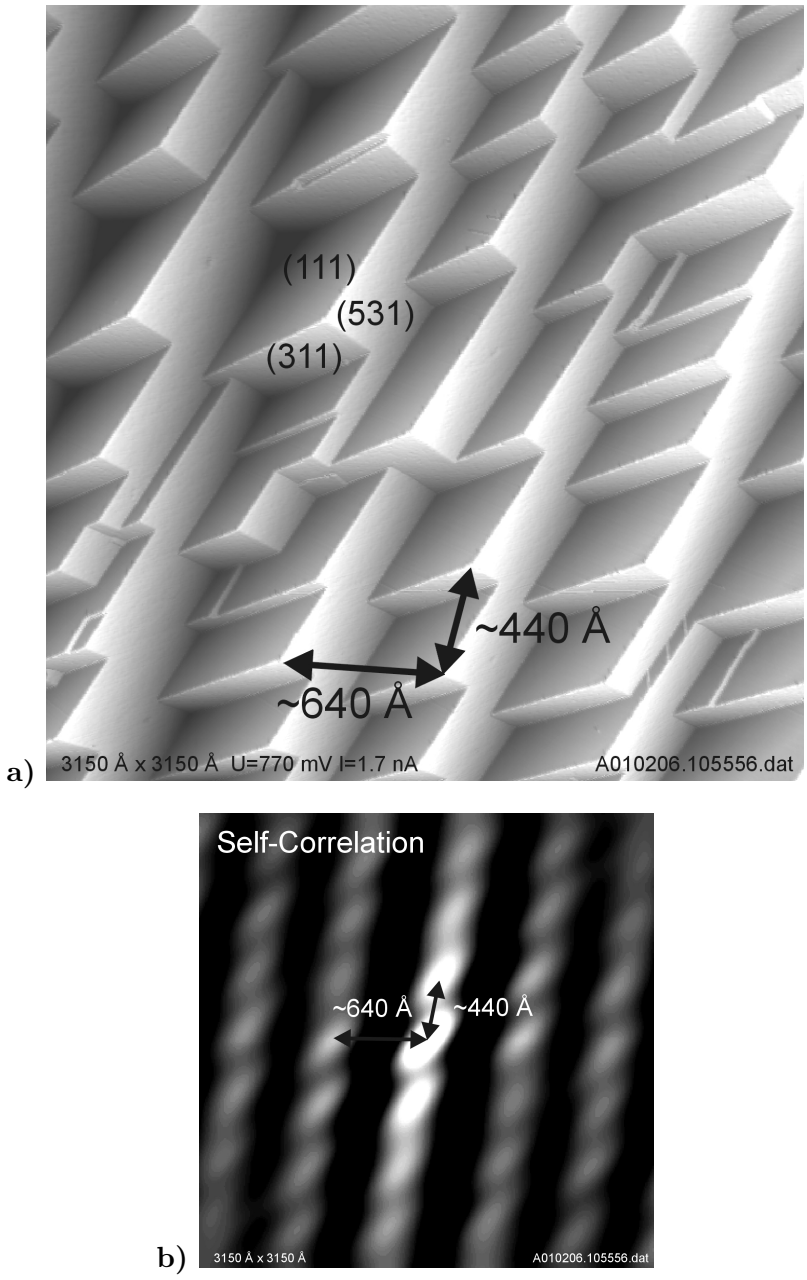

Figure 6.5: STM image and self-correlation function of the pyramidal facet structure after NaCl deposition at 600 K

a) STM image (3150 Å × 3150 Å, U=770 mV, I=1.7 nA) shows atomically flat facets; a comparison with the diffraction data allows to assign the facets to their respective orientations; the height modulation for this facet structure measures ∼80 Å

b) gray scale plot of the self-correlation function of the STM image from a); the periodicity of the facet structure can be seen; the separation is ∼440 Å along the staircase-like structure parallel to the $[\bar{3}50]$ direction and ∼640 Å perpendicular to it

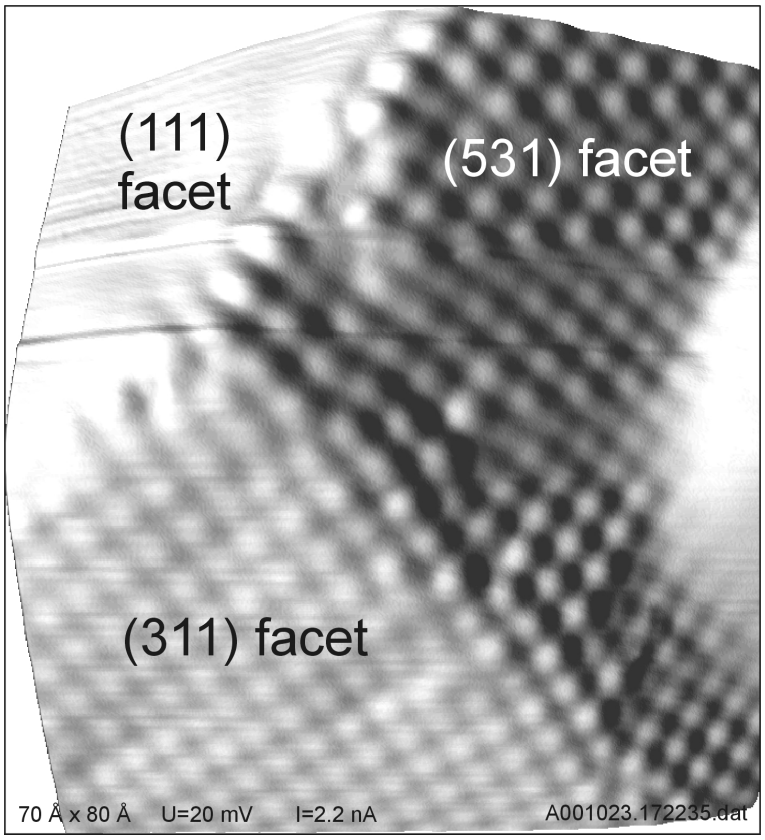

Figure 6.6: atomically resolved STM image (70 Å × 80 Å, U=20 mV, I=2.2 nA) of the three facets; clearly recognizable is the corrugation on the (311) and (531) facet, whereas the (111) facet appears atomically flat

and the shifted image are, the higher the value of the self-correlation function at a given shift (k1,k2). Consequently, the highest value is obtained at the center of the image (where k1 and k2 are zero). Any periodicity in the original image will be shown as a periodic pattern in the self-correlation. The periodicity of the STM image (cf. Figure 6.5a) along and perpendicular to the staircase-like structures can be clearly seen in the self-correlation image. As a result, for a substrate temperature of 600 K, equivalent facets have a spacing of ∼440 Å along the staircase-like structure parallel to the $[\overline{3}50]$ direction and of ∼640 Å perpendicular to this direction. For a lower substrate temperature of 500 K the spacing decreases to ∼250 Å × ∼400 Å. In the STM image, it is striking that the (311) and (111) facets are rather localized, whereas the (531) facets are extended over a wide range along the $[\overline{3}50]$ direction. The reason for this observation is the stabilization of this facet with a basically strain-free NaCl adlayer, which will be shown later. In Figure 6.6 one can see an atomically resolved STM image of all three facet orientations. The (111) facet appears completely flat, which suggests that no deposit is found on this facet. The

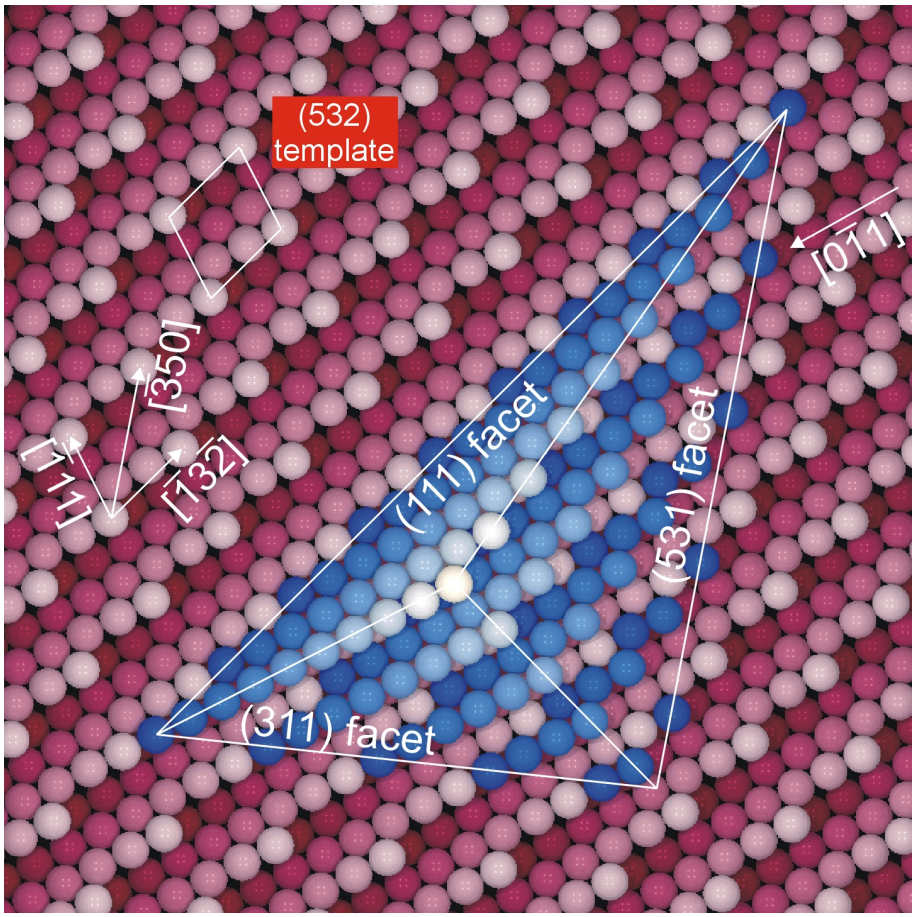

Figure 6.7: Hard-sphere model of the pyramidal structure
the orientation of the model is identical to the STM images shown; the pyramid is constructed by incorporating additional Cu atoms along the [0$\bar{1}$1] direction; for clarity, the steps in the (531) facet as well as the NaCl adlayer are omitted in this model

(311) and the stepped (531) facets, on the other hand, show a significant corrugation indicating that these facets are covered with NaCl.

The faceted surface geometry is illustrated by a hard-sphere model in Figure 6.7, where the azimuthal orientation is equivalent to the STM images. The facets are built up by incorporating additional Cu atoms along the [0$\bar{1}$1] direction. For clarity, the steps of the (531) surface and the NaCl adlayer are omitted in this model. The atomic surface structure of the three facet types can be recognized in this model (compare with the specific hard-sphere models in Figures 3.1b and 3.4).

The three facets will be investigated in greater detail with STM and SPA-LEED data in the following.

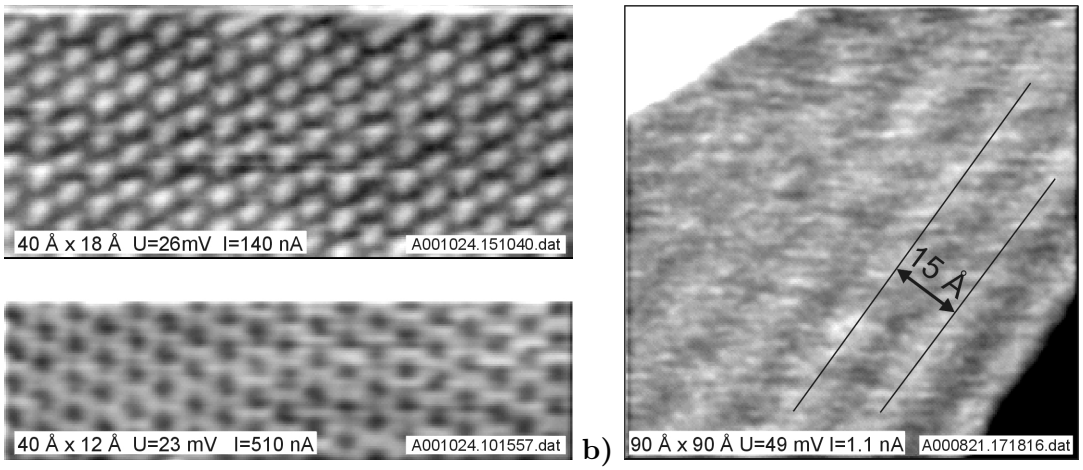

Figure 6.8: STM images of the (111) facet
a) atomically resolved STM images (top: 40 Å × 18 Å, U=26 mV, I=140 nA; bottom: 40 Å × 12 Å, U=23 mV, I=510 nA) of the (111) facet; recognizable is the hexagonal structure of the bare (111) facet
b) STM image (90 Å × 90 Å, U=49 mV, I=1.1 nA) shows the standing wave pattern, which is caused by the surface state of the (111) facet; the wavelength is ∼15 Å

(111) Facet

The Cu(111) surface is a close-packed surface with a nearest-neighbor distance of 2.55 Å. As mentioned above, this facet appears completely flat without any corrugation when imaged at typical tunneling parameters with a tunneling resistance in the range between 1 MΩ and 10 GΩ. To map the weak corrugation of a close-packed metal surface, a special tip-sample configuration is necessary. Molecules or metal atoms can be used to show this low corrugation by a type of lateral manipulation process [SE91, Mey96, MBR98]. Under such conditions the scan lines of STM images are lateral manipulation curves while pushing or pulling an adsorbates along the scan direction. Another possibility is the specific modification of the tip by transferring a molecule to the apex of the tip. For the STM images shown here, the first technique was used, but it is not known what kind of atom or molecule was used to map the surface corrugation. The resulting images with atomic resolution can be seen in Figure 6.8a. For these images it is not known if the protrusions in the upper image or the depletion in the lower image of Figure 6.8a are identical to the positions of the surface atoms. To solve this problem, one needs to know, at least, the kind of adsorbate, which was used for imaging this (111) facet. Nevertheless, in both cases the surface geometry is clearly recognizable as a close-packed structure identical to the (111) surface geometry. In addition, line scans were taken in both images to determine the nearest-neighbor distance. The values obtained correspond to the expected value of 2.55 Å

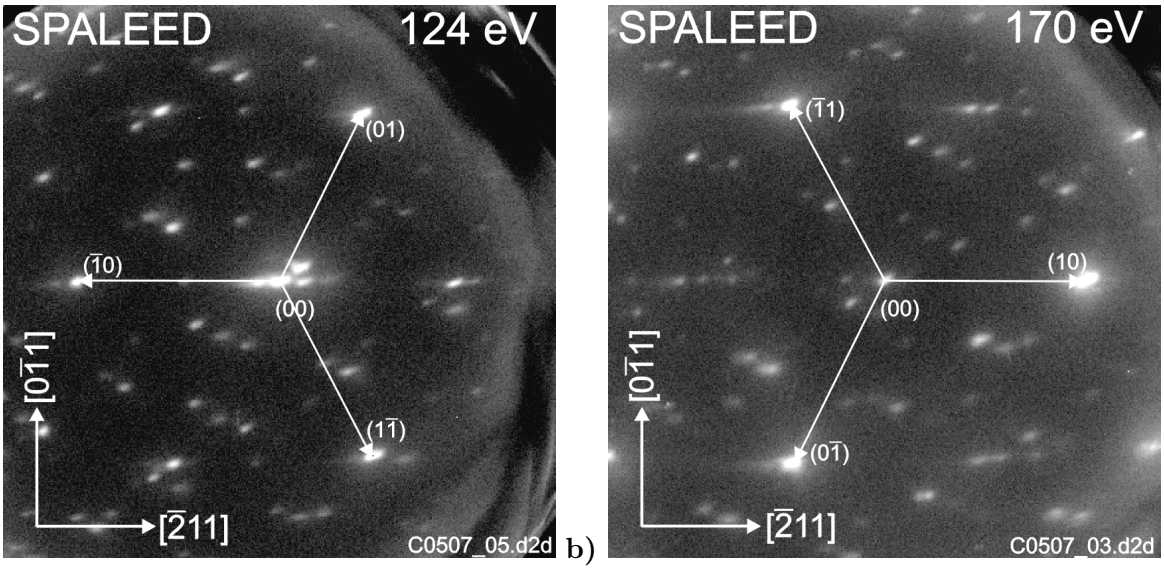

a) b)

Figure 6.9: Diffraction patterns of the (111) facet
only the spots belonging to the Cu(111) facets are fixed in their position with respect to $k_{\parallel}$ when changing the electron energy
a) diffraction pattern taken at 124 eV, which is close to the Bragg point energy for the spots at the (01), the $(\bar{1}0)$, and the $(1\bar{1})$ position
b) diffraction pattern taken at 170 eV, which is close to the Bragg point energy for the spots at the (10), the $(\bar{1}1)$, and the $(0\bar{1})$ position

within the uncertainty for STM length determinations.

Another feature of the Cu(111) surface can be observed on the facet (Figure 6.8b) for tunneling voltages close to the Fermi energy. This STM image shows the direct observation of a standing-wave pattern in the local density of states of the Cu(111) facet. These spatial oscillations are quantum-mechanical interference patterns caused by scattering of the two-dimensional electron gas off the edges of the facet. The wavelength of the surface state electrons at the Fermi energy (the energy probed by the STM in case of a small sample voltage) equals approximately 14 inter-atomic distances [Zan88]. Since the STM is sensitive to the square of the wave function, both maxima and minima of the wave function are seen as maxima of the current or the apparent height in the STM image. Subsequently, the wavelength observed with the STM is only half as long. In the present case, the wavelength is determined as about 15 Å, which is in perfect agreement with previous measurements on a Cu(111) surface (e.g. [CLE93]). These findings indicate that the (111) facet is uncovered, that means still bare copper.

To confirm these results for the (111) facet, diffraction data will be used which yield information averaged over the whole surface area. To investigate the (111) facet with SPA-LEED, the sample is adjusted in such a way that the incident wave vector component $k_{\perp}$ is normal to the

facet. As a result, the spots belonging to the (111) facet are fixed in their position with respect to $k_{\parallel}$ when changing the electron energy, whereas the position of spots belonging to other facet orientations are energy dependent.

For the (111) facet two exemplary diffraction patterns at different energies are seen in Figure 6.9. Each energy is close to the Bragg condition for one set of equivalent first order spots (cf. Table A.4). Over a wide energy range, only (111) spots belonging to the bulk terminated (1 × 1) configuration with a distance of 2.84 $Å^{-1}$ from the specular spot are observed. This distance in reciprocal space corresponds to 2.55 Å in real space, which is the nearest-neighbor distance of the Cu(111) surface. Since there are no other spots observed which are fixed in their position with respect to $k_{\parallel}$ while changing the electron energy, the diffraction data indicate that there is no NaCl overlayer on this facet. The results from the STM images and the analysis of the diffraction patterns lead to the conclusion that the (111) facet is a bare copper facet.

(311) Facet

The next facet investigated is the (311) facet, whose hard-sphere model can be seen in Figure 3.1b. The results discussed in section 5.1 have shown that KCl deposition on Ag(211) leads to the formation of (311)-oriented facets. These facets are stabilized by a (100)-terminated alkali halide layer, whose structural and orientational features turned out to be very similar to those found for NaCl layers grown on the Cu(311) substrate (cf. discussion in section 4.1). In the following the growth of NaCl on the (311) facets belonging to the pyramidal structure is compared to these related results discussed above.

The diffraction pattern in Figure 6.10 was recorded by adjusting the sample in such a way that the scattering component $k_{\perp}$ is parallel to the normal of the (311) facet. The features of this diffraction pattern are equivalent to those found for 1 ML NaCl on the Cu(311) substrate (cf. Figure 4.2a and discussion in the respective section 4.1): NaCl adlayer-induced spots in c(2 × 2) configuration, spots belonging to the NaCl(100) bulk terminated p(1 × 1) configuration, and a spot splitting parallel to the intrinsic steps of the Cu(311) facet in $[01\bar{1}]$ direction. The resulting structure of the NaCl adlayer and its arrangement relative to the Cu(311) substrate can be seen in the hard-sphere model in Figure 6.11[1]. The essential features are an alignment of the polar ⟨110⟩ in-plane directions of the NaCl film parallel and perpendicular to the intrinsic Cu steps and a pinning of the Cl ions by these steps. The Cl-Cl distance perpendicular to the steps is thus equal to the intrinsic step separation of 4.23 Å. Along the intrinsic steps, domains of two locally commensurate configurations with a c(2 × 2) and a p(1 × 1) symmetry alternate.

[1]This hard-sphere model is identical to that shown in Figure 4.3. For convenience it is reproduced in this context to compare with the present data

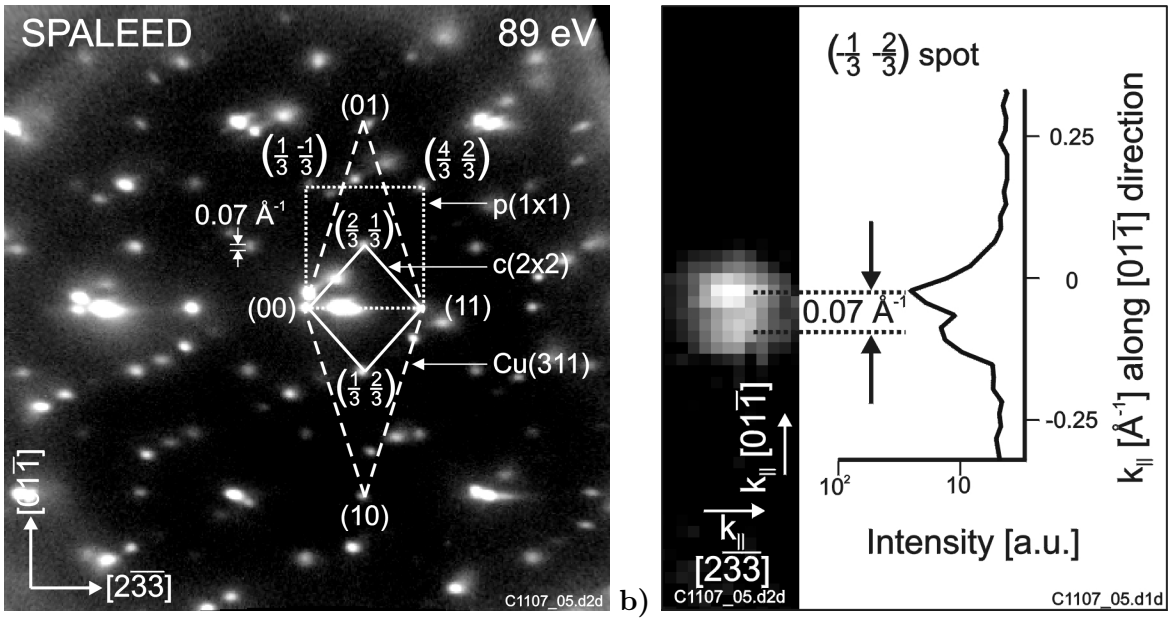

Figure 6.10: Diffraction pattern and line scan of the NaCl-covered (311) facet
a) spots for bulk-terminated NaCl(100) p(1 × 1) configuration (dotted line) and the NaCl adlayer-induced c(2 × 2) configuration (solid line); also indicated is the unit cell of Cu(311) (dashed line)
b) line scan of the $(-\frac{1}{3} - \frac{2}{3})$ spot along $[01\bar{1}]$ direction; the spot splitting measures $0.07\,\text{Å}^{-1}$ parallel to the intrinsic steps

The separation between adjacent domains of identical symmetry is given by the spot splitting of $0.07\,\text{Å}^{-1}$ (cf. line scan in Figure 6.10b), which corresponds to a distance of ∼90 Å. The average Cl-Cl distance is 3.88 Å along the intrinsic steps for an expansion with respect to a perfectly commensurate configuration and 3.77 Å for a contraction.

Complementary STM data for the (311) facet will be presented in the following. An atomically resolved STM image of the (311) facet can be seen in Figure 6.12a. The orientation of the Cu(311) template can be inferred from the hard-sphere model in Figure 6.7. It shows that the close-packed Cu rows in $[01\bar{1}]$ direction run diagonal from the lower left corner to the upper right corner. The structure seen in the STM image corresponds to a square surface unit cell, which is not equivalent to the surface symmetry of Cu(311). Apparently, the (100)-oriented NaCl overlayer is imaged by the STM. The size of the unit cell measuring about 4 Å × 4 Å indicates that just one species of the alkali halide adlayer is imaged as protrusion by the STM. Previous measurements and calculations of Hebenstreit et al. [HRH+99] and Repp et al. [RFMR01] show that only Cl ions are imaged as protrusions. In this STM image, the previously described existence of two different configurations, c(2 × 2) and p(1 × 1), is not observed. However, these features

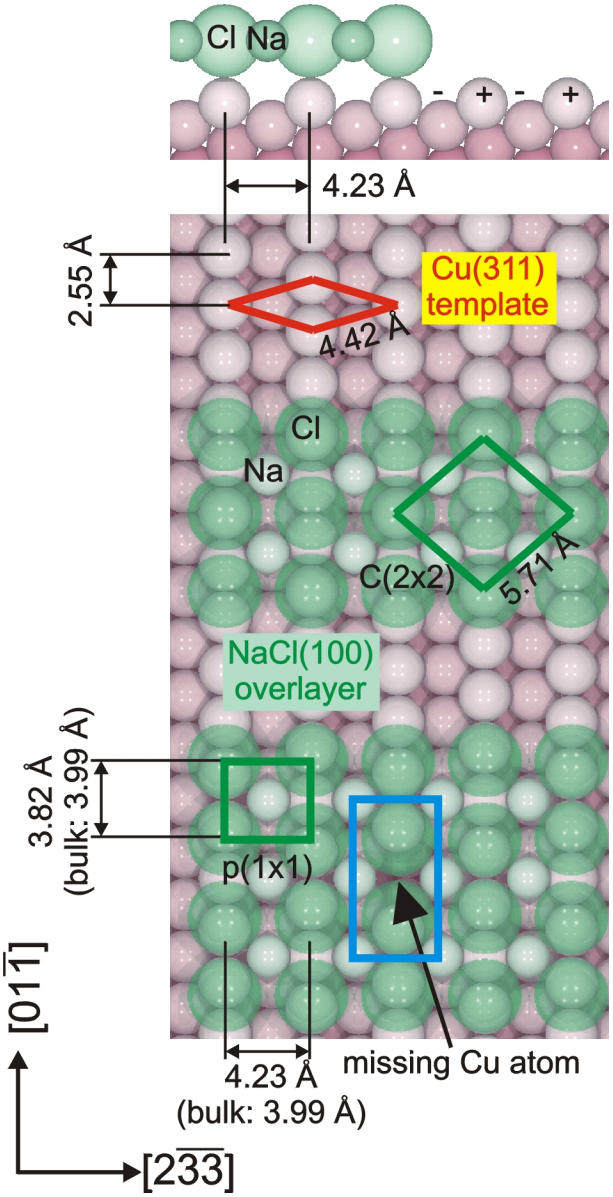

Figure 6.11: Hard-sphere model of the NaCl configuration on the (311) facet
top: side view of the charge modulated (311) surface with the Cl ions pinned to the top of the intrinsic Cu steps
middle: NaCl in c(2 × 2) configuration with the Cl ions located in alternating on-top and bridge positions with respect to the underlying Cu atoms
bottom: NaCl in a p(1 × 1) configuration, which is shifted by $\frac{1}{4}$ of a Cu-Cu spacing with respect to the c(2 × 2) configuration along the intrinsic steps; this arrangement leads for all Cl ions to equivalent vertical positions
blue rectangle: missing Cu atom in the interface, which causes the neighboring Cl ions to change their vertical and lateral position (cf. Figure 6.12b and c)

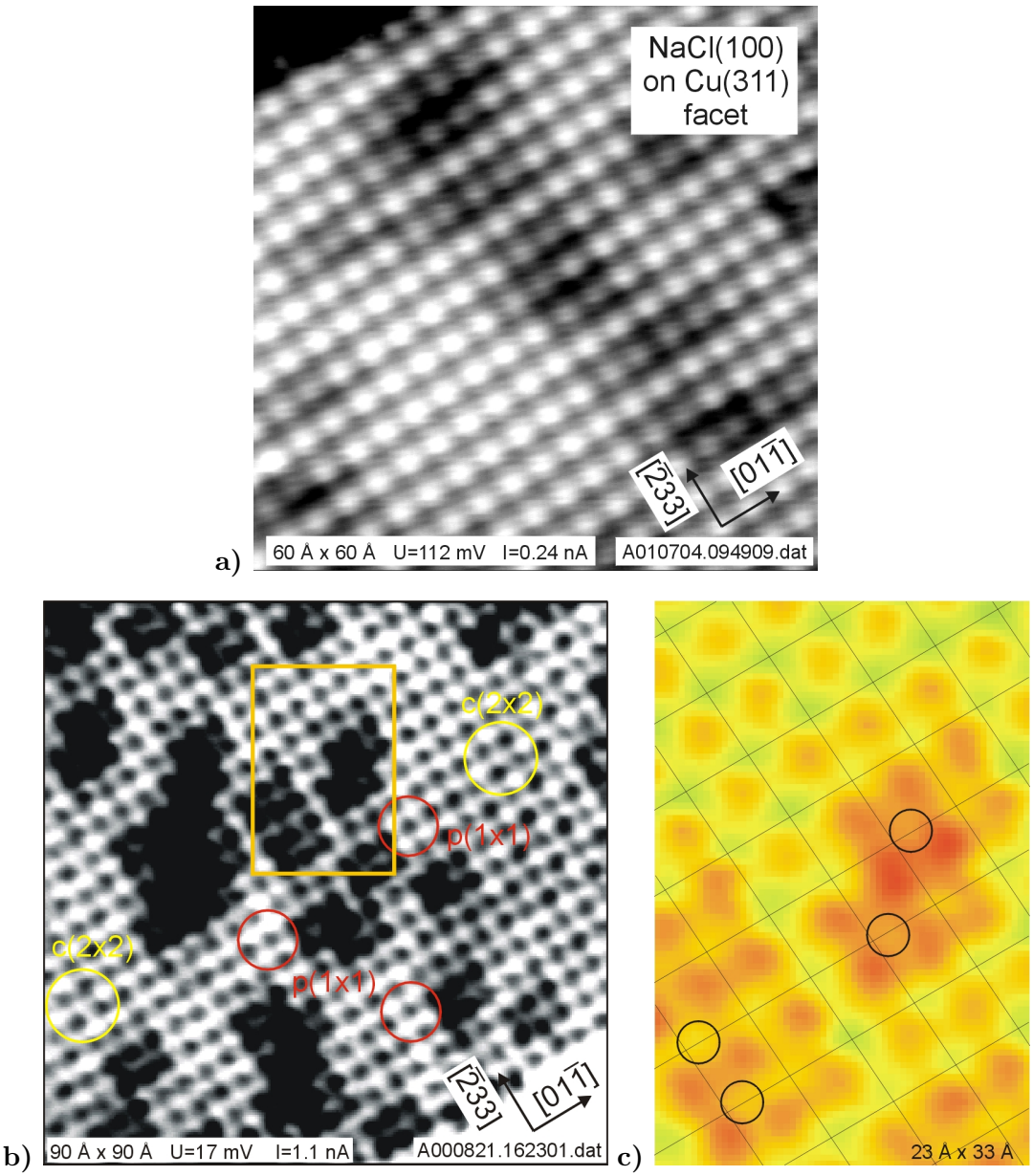

Figure 6.12: Atomically resolved STM images of the NaCl-covered (311) facet
a) 60 Å × 60 Å, U=112 mV, I=0.24 nA; the size of the unit cell of about 4 Å × 4 Å belongs to NaCl in (100) orientation, where only one species (the Cl ions [HRH^+99]) is mapped by the STM
b) 90 Å × 90 Å, U=17 mV, I=1.1 nA; NaCl in p(1 × 1) (red circles, middle) and c(2 × 2) configuration (yellow circles, left and right)
c) 23 Å × 33 Å; color-coded, yellow part of the STM image in b); colors scale from red over yellow to green with increasing height; interface defects cause the indicated Cl ions to change their lateral and vertical position with respect to the p(1 × 1) configuration (indicated by the grid lines)

are indeed recognized in the STM image in Figure 6.12b. Here, the alternation of domains with c(2 × 2) configuration (yellow circles, lower left and upper right) and p(1 × 1) configuration (red circles, center) can be observed along the $[01\bar{1}]$ direction, i.e. parallel to the intrinsic steps. The mean spacing of equivalent domains averaged over the whole surface is ∼90 Å as deduced from the LEED data (cf. Figure 6.10b).

Another interesting feature seen in the atomically resolved STM image are the dark regions (cf. Figure 6.12b). These defects were also found, when investigating the growth of NaCl on a Cu(311) substrate by STM [RFMR01]. In that study as well as in the present case, these defects occur only in areas, where the NaCl adlayer is in the p(1 × 1) configuration. An explanation that meets both the symmetry of the defect itself as well as the symmetry of its lateral position is that a Cu atom is missing in the underlying (311) facet [RFMR01] (cf. blue square in the hard-sphere model in Figure 6.11). This explanation is reasonable also for the present case, where a lateral and vertical shift of the Cl ions at these defects could be observed (cf. Figure 6.12c). The Cl ions marked by a circle deviate from the lateral position of the p(1 × 1) configuration, which is indicated by the grid lines. Here, these defects occur more frequently since the mass transport for building up the present facet structure is evidently much higher than the mass transport required to flatten the interface between the adlayer and the template when growing NaCl on the Cu(311) substrate.

To conclude, the diffraction data reveal that the Cu(311) facet is overgrown by a (100)-terminated NaCl layer, whose orientation is in accordance with that observed for the system NaCl/Cu(311) (see section 4.1). The two locally commensurate configurations, a c(2 × 2) and a p(1 × 1) configuration, could be identified by the STM measurements. The Cl ions are pinned by the Cu steps, which causes a Cl-Cl distance of 4.23 Å perpendicular to the step direction. Along the intrinsic steps a relaxed Cl-Cl distance is achieved by the alternation of domains with c(2 × 2) and p(1 × 1) configuration.

Stepped (531) Facet

The third facet type which builds up the pyramidal structure on Cu(532) is a stepped (531) facet. Similar to the original (532) surface, the (531) surface is a kinked surface, a hard-sphere model can be seen in Figure 3.4. The surface unit cell is a rhombus with 4.42 Å side length and an angle of 80.4° between the $[\bar{1}2\bar{1}]$ and the $[\bar{1}12]$ direction. Hence, the (531) surface is an open surface, for which a surface charge smoothing effect occurs due to the Smoluchowski effect [Smo41]. As a result, a depletion of electrons (i.e. a positive charge) occurs at the kink atom positions, whereas an accumulation of electron charge is centered between the kink atoms. Due to this charge modulation a strong Coulomb interaction between the surface and the ionic

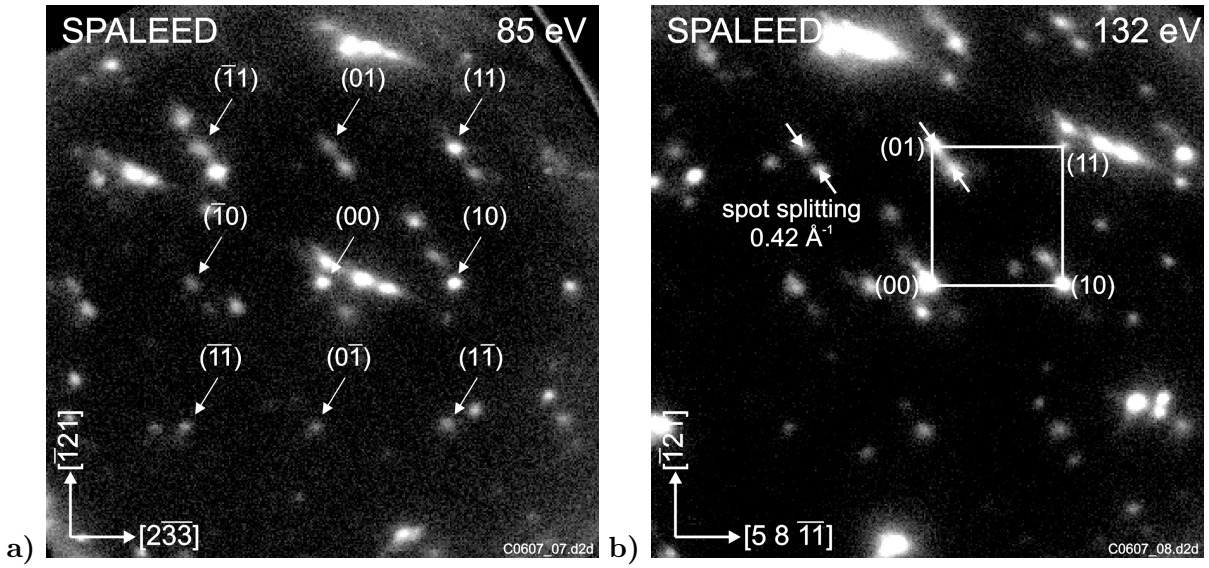

Figure 6.13: Diffraction pattern of the NaCl-covered (531) facet
spots fixed in their position with respect to $k_{\parallel}$ belong to NaCl (100) adlayer and a superstructure (spot splitting)
a) diffraction pattern taken at 85 eV; the spots are labeled according to the NaCl adlayer
b) diffraction pattern taken at 132 eV with the NaCl(100) surface unit cell; the superstructure (periodic arrangement of regular defect steps in the (531) template) is causing the spot splitting of $0.42\,\text{Å}^{-1}$

insulator NaCl can be expected. A commensurate NaCl adlayer with the Cl ions pinned to the kink atoms would cause a sheared unit cell with tensile strain of about 11% along both polar $\langle 110 \rangle$ in-plane directions. Because of the geometrical mismatch, such a configuration would be energetically unfavorable.

The diffraction patterns in Figure 6.13 were taken with the scattering vector component $k_{\perp}$ normal to the stepped (531) facet. In these diffraction patterns two features can be observed: The spots labeled indicate the p(1 × 1) symmetry of the NaCl adlayer in (100) orientation. The corresponding square unit cell is shown in Figure 6.13b. The size of this unit cell is $1.52\,\text{Å}^{-1} \times 1.54\,\text{Å}^{-1}$ in reciprocal space, which corresponds to $4.13\,\text{Å} \times 4.08\,\text{Å}$ in real space. These values are significantly smaller than the distance between the kinks (4.42 Å in both direction) of the (531) surface. The second feature observed is a spot splitting of $0.42\,\text{Å}^{-1}$, which corresponds to 15 Å in real space. This spot splitting indicates the formation of a periodic array of defect steps in the underlying Cu(531) template, which allows for a reduction of the strain in the alkali halide layer. Such a mechanism for the relief of epitaxial strain has been also observed for the previously described systems NaCl/Cu(311), KCl/Cu(311), and NaCl/Cu(221) discussed in chapter 4, where defect steps were incorporated to reduce the strain perpendicular to the

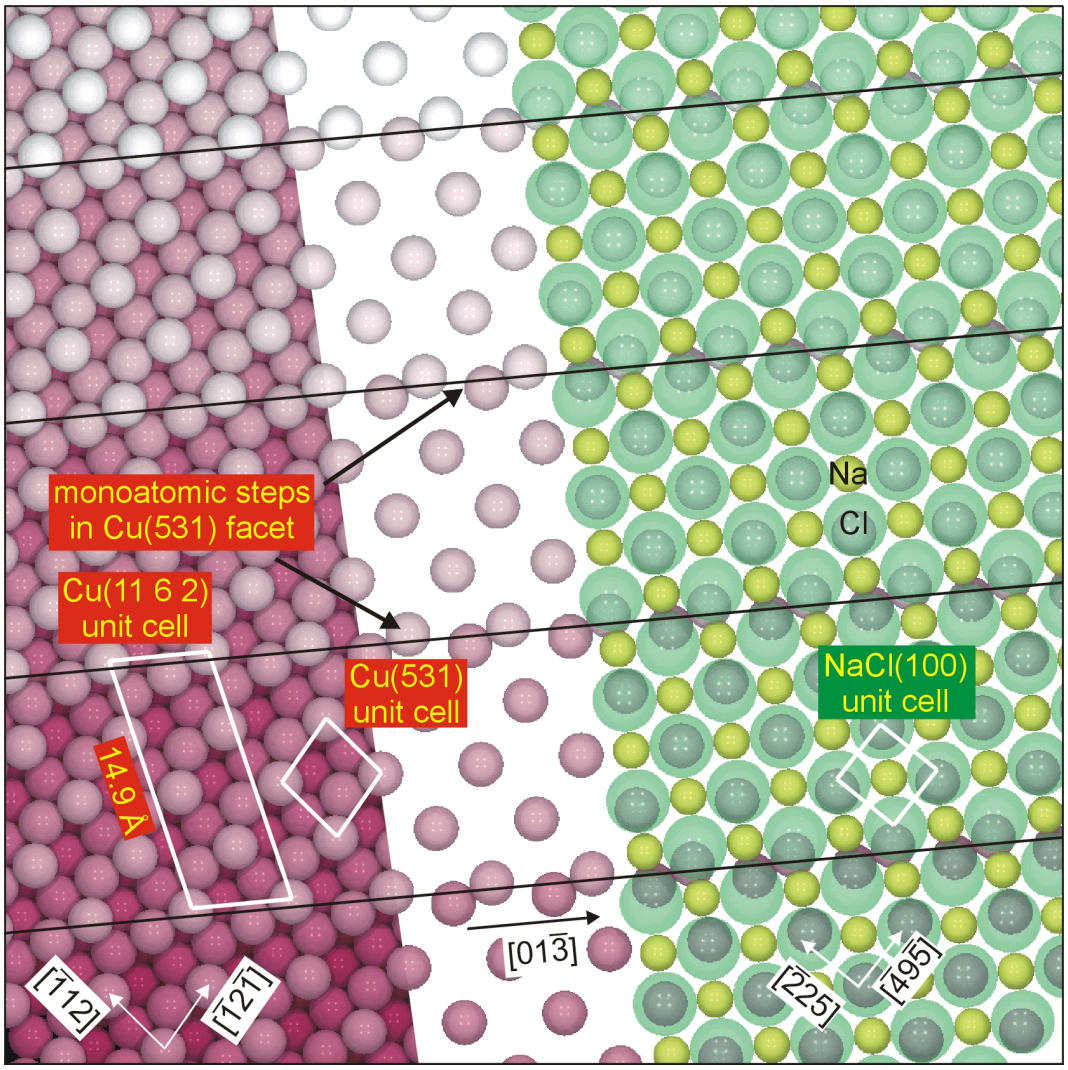

Figure 6.14: Hard-sphere model of the NaCl configuration on the stepped (531) facet
left: (531) oriented terraces (diamond-shaped unit cell, side length: 4.42 Å, angle: 80.4°), which are separated by monoatomic defect steps running parallel to the [01$\bar{3}$] direction (black, almost horizontal lines) in a distance of ∼15 Å; resulting overall facet orientation is (11 6 2) (parallelogram-shaped unit cell, side length: 14.9 Å × 5.71 Å, angle: 103.3°)
middle: only the top-most kink atoms which carry a positive charge due to the Smoluchowski effect are drawn into the model
right: NaCl in (100) orientation; the polar close-packed Cl ion rows are parallel to the [$\bar{2}$25] and the [4$\bar{9}\bar{5}$] direction; the positions of the Cl ions are optimized on this stepped (531) facet in such a way that the overlap with the kink atoms is maximized (energetically favorable position due to the Smoluchowski effect); the Cl-Cl distance is 4.14 Å along the [$\bar{2}$25] direction and 3.99 Å along the [4$\bar{9}\bar{5}$] direction, which is reasonable close to bulk value of 3.99 Å; the resulting angle of the NaCl surface unit cell in this configuration is 89.1° (bulk: 90°)

intrinsic steps of the Cu template. The direction and size of the spot splitting is consistent with the incorporation of monoatomic defect steps parallel to the $[01\overline{3}]$ direction with a separation of 14.4 Å. This arrangement leads to a surface, which can be described by the Miller indices (11 6 2).

The configuration, which is extracted from the SPA-LEED data, can be seen in the hard-sphere model of Figure 6.14. On the left hand side of this figure, the stepped Cu(531) surface is illustrated. In this model, the surface unit cells of the (531) and the (11 6 2) surface orientations are plotted. For clarity, the middle and the right part contain only the top-most kink atoms of the Cu template (the latter is supposed to carry a positive charge due to the Smoluchowski effect). The monoatomic steps indicated by almost horizontal lines are downward steps when moving from the top to the bottom. In the present case, the result of a monoatomic defect step is that the kink atom positions of neighboring terraces are shifted vertically and laterally against each other. This is important for the adjustment of the NaCl adlayer relative to the stepped (531) template. The right hand side of Figure 6.14 shows a coincident matching between an almost strain-free NaCl (100) film and the stepped (531) facet, where the Cl ions are located close to the position of the kink atoms. The distance between two equivalent Cl ions is 19.94 Å along the $[\overline{4}9\overline{5}]$ direction and 20.74 Å along the $[\overline{2}25]$ direction. This results in Cl-Cl distances of 3.99 Å and 4.14 Å with an angle of 89.1° between the two directions in close agreement with the unit cell dimensions extracted from the SPA-LEED data. Comparing these values with the bulk values of NaCl (square surface unit cell with side length of 3.99 Å), it is evident that this configuration leads to a basically strain-free adlayer on the stepped Cu(531) facet.

This model is corroborated by the STM data of the stepped (531) facet. An atomically resolved STM image can be seen in Figure 6.15a. One can clearly recognize the (100)-like NaCl overlayer, where, like for the Cu(311) facet, only the Cl ions are imaged by the STM. The bright, almost horizontal rows of Cl ions indicate the monoatomic steps in the underlying template, which are separated by about 15 Å. The line scan (Figure 6.15b) taken along a close-packed Cl ion row shows the described configuration in the hard-sphere model: Moving along the close-packed Cl ion rows, a monoatomic step occurs every 5 Cl-Cl spacings. The height variation of the undulation is determined as ∼0.19 Å, which is significantly smaller than the height of 0.61 Å for a defect step of the (531) facet. This suggests a carpet-like growth mode, which is commonly observed for the growth of alkali halides on surfaces with defect steps [HRH$^+$99, SSP93]. From the Cl-Cl distance in the STM image, the size of the NaCl square unit cell can be determined as ∼4 Å in side length. This is in good agreement with the described configuration. On the other hand, it is evident from the STM image that the assumption of a strictly regular array of straight defect steps is an idealized model. In the real case, the steps are more irregular than the model suggests, but the overall faceting mechanism can be explained in this way. Also in

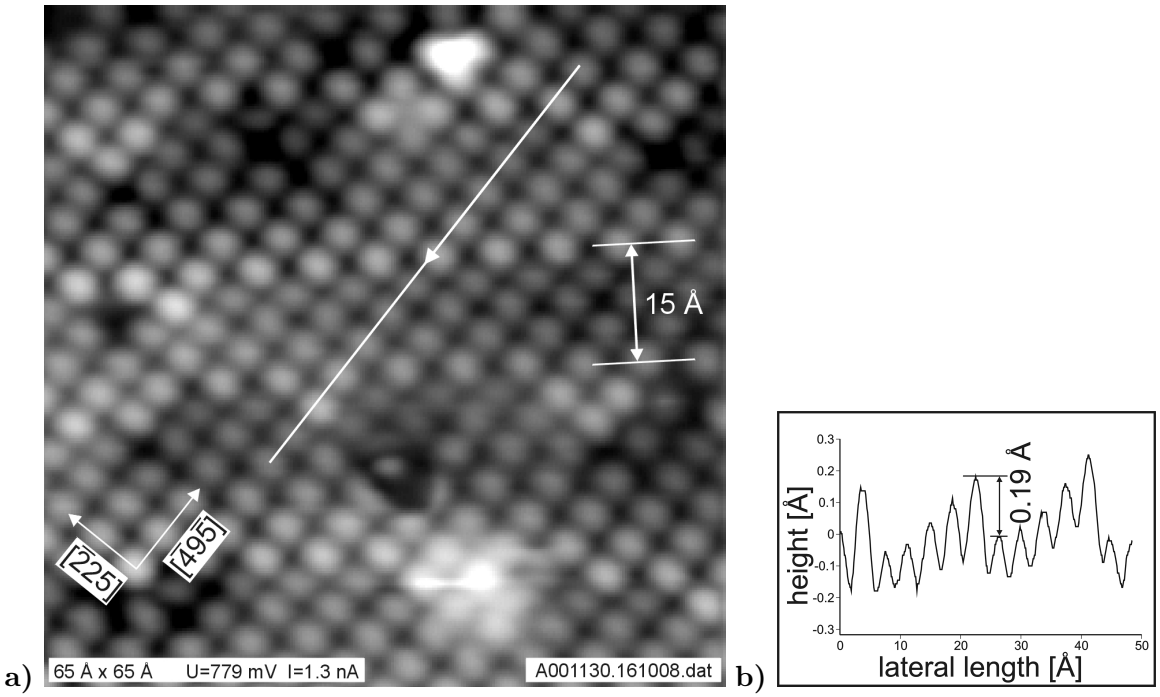

Figure 6.15: STM image with line scan of the NaCl-covered (531) facet
a) atomically resolved STM image (65 Å × 65 Å, U=779 mV, I=1.3 nA) of the NaCl-covered (531) facet; visible are the horizontal lines of Cl ions with higher protrusion, which are caused by defect steps in the underlying (531) facet; Cl-Cl distance ∼4 Å
b) line scan taken in a) from the top to the bottom; steps down occur every 5 Cl ions; the height variation of 0.19 Å is significantly smaller than the monoatomic defect step height of 0.61 Å, which suggests a carpet-like growth mode for the NaCl layer

the present case, the overall interfacial arrangement is ruled by the energetic attempt to achieve a geometrical matching between the charge-modulated (531) facet and the ionic insulator film, which causes the incorporation of defect steps into the template facet.

To summarize, the STM measurements and the SPA-LEED data show that the Cu(531) facet is overgrown by a single monolayer of a (100)-oriented NaCl film. The mismatch between the geometry of the Cu(531) surface and a (100)-terminated NaCl adlayer is overcome by incorporation of monoatomic defect steps at the interface, which was also observed for the previously investigated systems, e.g. 3 ML NaCl on the Cu(311) substrate. This incorporation of defect steps allows the NaCl layer to relax into a basically strain-free state with the Cl ions close to the lateral positions of the underlying kink atoms. A central result of this section can be formulated as follows: Also for kinked metal surfaces, there is an enhanced binding between charge-modulated substrates and ionic insulators.

6.2 Chemical Selectivity

The previously described prestructured surface was used to verify and utilize the different chemical reactivity of the different facets. These experiments were carried out (i) by adsorbing carbon monoxide (CO) and (ii) by evaporating silver (Ag) onto the pyramidal surface structure. The results of both approaches will be shown in the following.

6.2.1 CO Adsorption

For molecular adsorption experiments on the facet structure carbon monoxide was chosen. According to previous studies reported in the literature, the binding energies for CO on the NaCl(100) surface are about three times larger compared to those for CO on Cu(111). For CO on Cu(111), Conrad et al. [CEKL75] estimated an adsorption energy of about -50 kJ/mol. The adsorption energy of CO on the NaCl(100) surface was the object of different studies. In a theoretical work Mahmud et al. [MD95] determined a value of -11 kJ/mol with ab-initio Hartree-Fock self-consistent field calculations, whereas experimental studies by Hardy et al. [HESS85] and Richardson et al. [RBE87] report a value of -14 ± 1 kJ/mol and -13 ± 3 kJ/mol, respectively. Furthermore, phase diagrams of the CO adsorption on NaCl(100) [HESS85] show that at a pressure of $1 \cdot 10^{-9}$ mbar and substrate temperatures higher than 60 K the adsorption on NaCl(100) results in a coverage lower than 5%, whereas CO adsorption on Cu(111) occurs at this conditions [CEKL75]. Therefore, comparable experimental conditions were chosen in the present case to verify the chemical selectivity of the facet structure.

As a starting template, a pyramidal surface structure was prepared onto Cu(532) as discussed in section 6.1 (i.e. ∼0.6 ML NaCl at 600 K). Subsequently, the surface was exposed to 8 Langmuir[2] CO at a sample temperature of 90 K. The overall surface topography obtained was identical to that without CO (cf. Figure 6.5a). Detailed STM observations performed with atomic resolution (cf. Figure 6.16a and b), on the other hand, show a difference in the atomic corrugation compared to an as-grown pyramid shown in Figure 6.6. Figure 6.16b is a Laplace-filtered image (see section 1.3.5 for image editing) of Figure 6.16a to simultaneously display the corrugation of all three facets with the same gray scale. The (311) and the (531) facet show similarly the corrugation of the NaCl (100) film. Obviously, these facets are passivated by the chemically inert NaCl adlayer. The (111) facet, which appeared smooth at comparable tunneling parameters before, shows a clear corrugation after the CO exposure, which indicates CO adsorption on this facet. Figures 6.16c and d show a magnification of the CO-covered (111) facet.

[2] d[Langmuir] $= 7.5 \cdot 10^5 \cdot p$[mbar] $\cdot\, t$[sec], with d as the dose, p as the pressure, and t as the exposure time

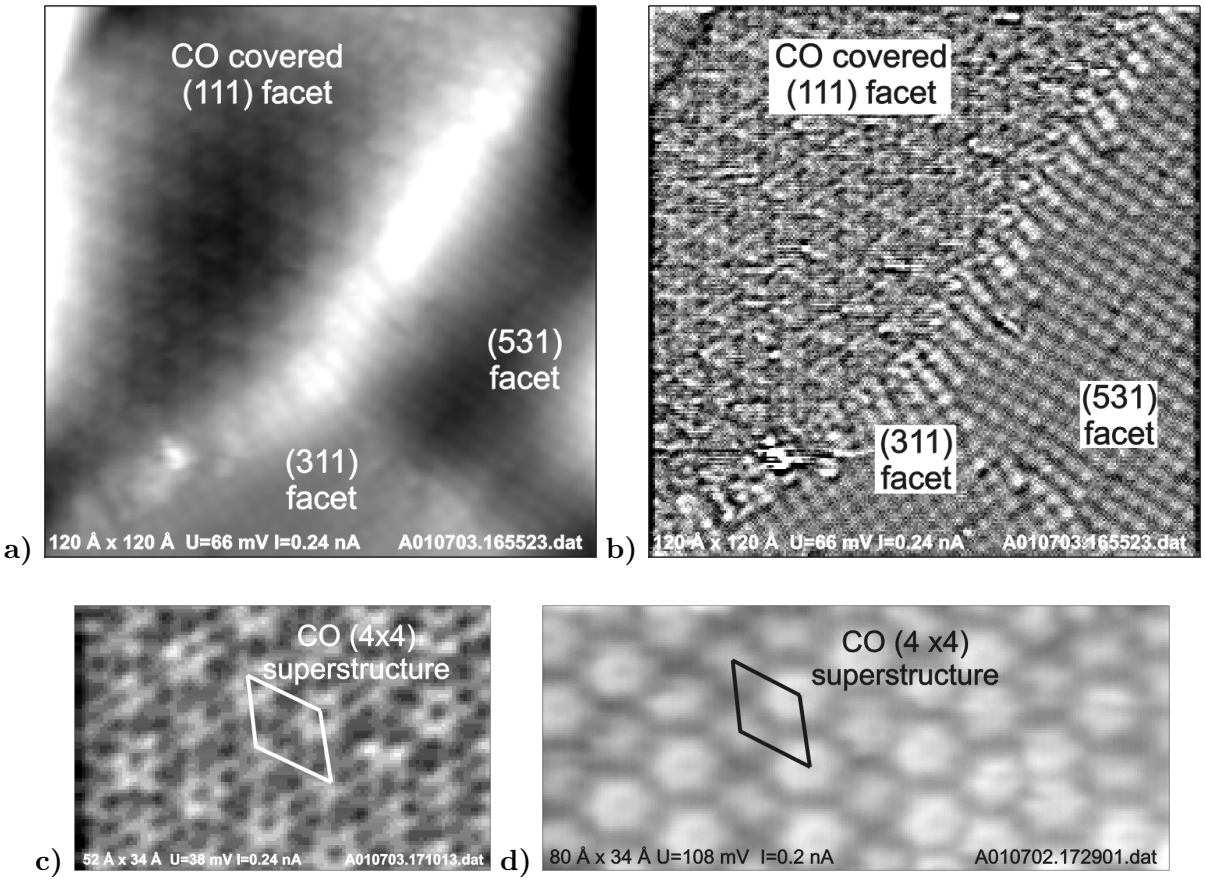

Figure 6.16: STM images of the faceted Cu(532) surface after adsorbing CO
a) STM image (120 Å × 120 Å, U=66 mV, I=0.24 nA) of a single pyramid
b) STM image in a) was Laplace-filtered to visualize the atomic corrugation on all three facets with the same gray scale; the (311) and the (531) facet show a corrugation indicative for NaCl(100) while the (111) facet exhibits a (4 × 4) superstructure with respect to the bare Cu(111) facet
c) STM image (52 Å × 34 Å, U=38 mV, I=0.24 nA) of the CO covered Cu(111) facet; the present tip condition reveals internal structures of the (4 × 4) CO superstructure
d) STM image (80 Å × 34 Å, U=108 mV, I=0.2 nA) of slightly varying (4 × 4) super cells imaged with a different tip condition

CO adsorption on the Cu(111) surface was previously investigated, for instance with LEED measurement by Hollins and Pritchard [HP79, Pri79] and with STM studies by Bartels et al. [BMR99]. The common result for the saturation coverage of CO at a sample temperature of 85 K is a (1.39 × 1.39) phase, whereas it was found that CO molecules bind to on-top and bridge sites, which causes a reconstruction into slightly varying (4 × 4) unit cells.

This superstructure can be observed in the STM images seen in Figures 6.16c and d. The imaging of the CO adlayer strongly depends on the apex of the STM tip. One can clearly see that the tip condition leading to the image in Figure 6.16c reveals more internal details of the (4 × 4) supercell than that evident from Figure 6.16d. The differences in the tip conditions occur while modifying the tip during the so-called tip forming, which means a controlled mechanical contact between tip and sample. The chemical properties of the tip are not known for either of the two STM images.

In conclusion, the chemical selectivity of the fabricated facet structure was demonstrated by preferred CO adsorption on the bare Cu(111) facets only. The (311) and the (531) facet, on the other hand, turn out to be chemically passivated under these conditions.

6.2.2 Ag Deposition onto the Facet Structure

After successfully using the chemically modulated facet structure for exclusively adsorbing molecules onto the Cu(111) facet, the next step was to verify whether the facet structure can be selectively decorated with a metal by means of selective nucleation. For this experiment Ag was chosen as the metallic deposit. Previous experimental investigations on the adsorption of Ag on Cu(111) are reported in the literature [MHC92, KMG95], whereas for the adsorption of Ag on a NaCl(100) surface there are only theoretical studies, e.g. [Mej96]. Recently, single Ag atoms deposited on a NaCl (100) film at 10 K were investigated in our group [Rep02].

The deposition of Ag onto the facet structure was performed at a sample temperature around 300 K with a coverage of ∼0.5 ML. The result can be seen in the STM image in Figure 6.17a and the Laplace-filtered duplicate in Figure 6.17b. Comparing these STM images with Figure 6.5a, it is obvious that the facets are no longer atomically smooth: All facets show a stepped structure. These steps indicate Ag aggregation on all facets. Equivalent results were obtained at various deposition parameters (e.g. different, especially lower sample temperatures). It will be shown in the following that Ag forms an incommensurate two-dimensional layer on the Cu(111) facets, while interfacial growth takes place between the NaCl adlayer and the Cu template on the Cu(311) and the Cu(531) facets. To visualize the facet structure, the stepped facets in the STM image were colored as shown in Figure 6.17c. The (111) facet consists of two terraces (yellow and green), whereas the green terrace is elevated compared to the yellow terrace, indicating the

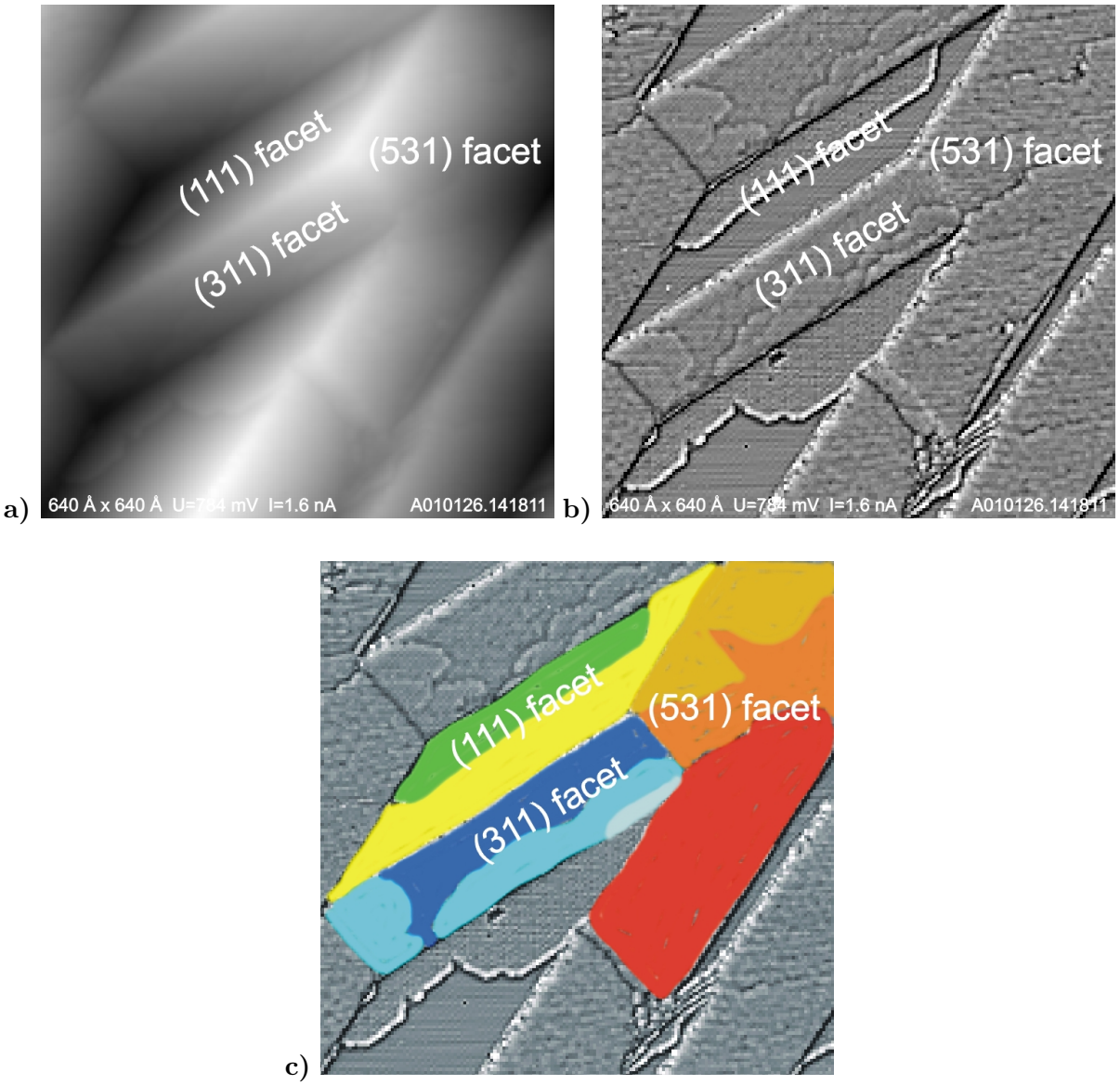

Figure 6.17: STM images of the faceted Cu(532) surface after deposition of Ag
a) STM image (640 Å × 640 Å, U=784 mV, I=1.6 nA)
b) Laplace-filtered STM image from a) to show the steps on all three facets caused by the Ag deposition
c) colored STM image from b) to clarify the different terraces on the facets; (111) facet: upper green and lower yellow terraces; (311) facet: light blue (high), blue (middle), and dark blue (low) terraces; (531) facet: red (high), orange (middle), and ocher (low) terraces

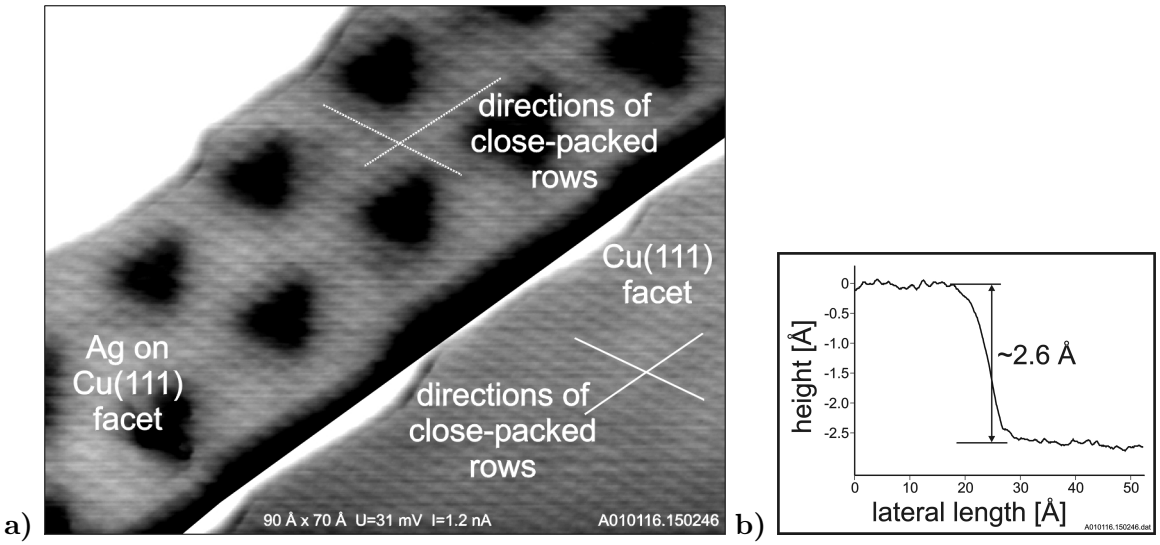

Figure 6.18: STM image and line scan of the (111) facet after the deposition of Ag at 300 K
a) STM image (90 Å × 70 Å, U=31 mV, I=1.2 nA); different gray scales used for the Cu(111) facet (right lower corner) and the Ag(111) island (middle) to show the corrugation in both parts; white, upper left corner corresponds to a (311) facet; two directions of the close-packed rows are indicated by the white lines; azimuthal difference in the orientation of the close-packed rows of Cu(111) and Ag(111) measures ∼1.3°
b) line scan taken over the step edge of the Ag island shows a step height of ∼2.6 Å

Ag adlayer on the (111) facet. The (311) facet has terraces with three different heights. The lowest terrace is marked dark blue, the middle one is blue, and the light blue terrace is the highest of the three. Steps separate these terraces, which are formed after the Ag deposition. The (531) facet exhibits steps as well which separate different terraces. Downward steps lead from the red to the orange terrace as well as from the orange to the ocher terrace. The terraces formed on the (531) facet are not strictly separated by steps, terraces of different height merge into each other. A detailed look at the three facets will be given in the following.

Ag on the Cu(111) Facet

On the previously flat Cu(111) facet the growth of an Ag island is clearly observed as shown in Figure 6.17. An STM image with atomic resolution of the Ag island and the Cu(111) facet can be seen in Figure 6.18a. In the image, two separate gray scales were chosen for the two surface areas to simultaneously display the features of both regions. The white part in the upper left corner corresponds to a (311) facet. The Cu(111) facet and the Ag island show the expected hexagonal symmetry. The ratio of the nearest-neighbor distances between both areas was determined to 1.14, which is close to the ratio of the bulk values $\frac{a_{0,Ag}}{a_{0,Cu}}$=1.13. The lines indicate the directions of

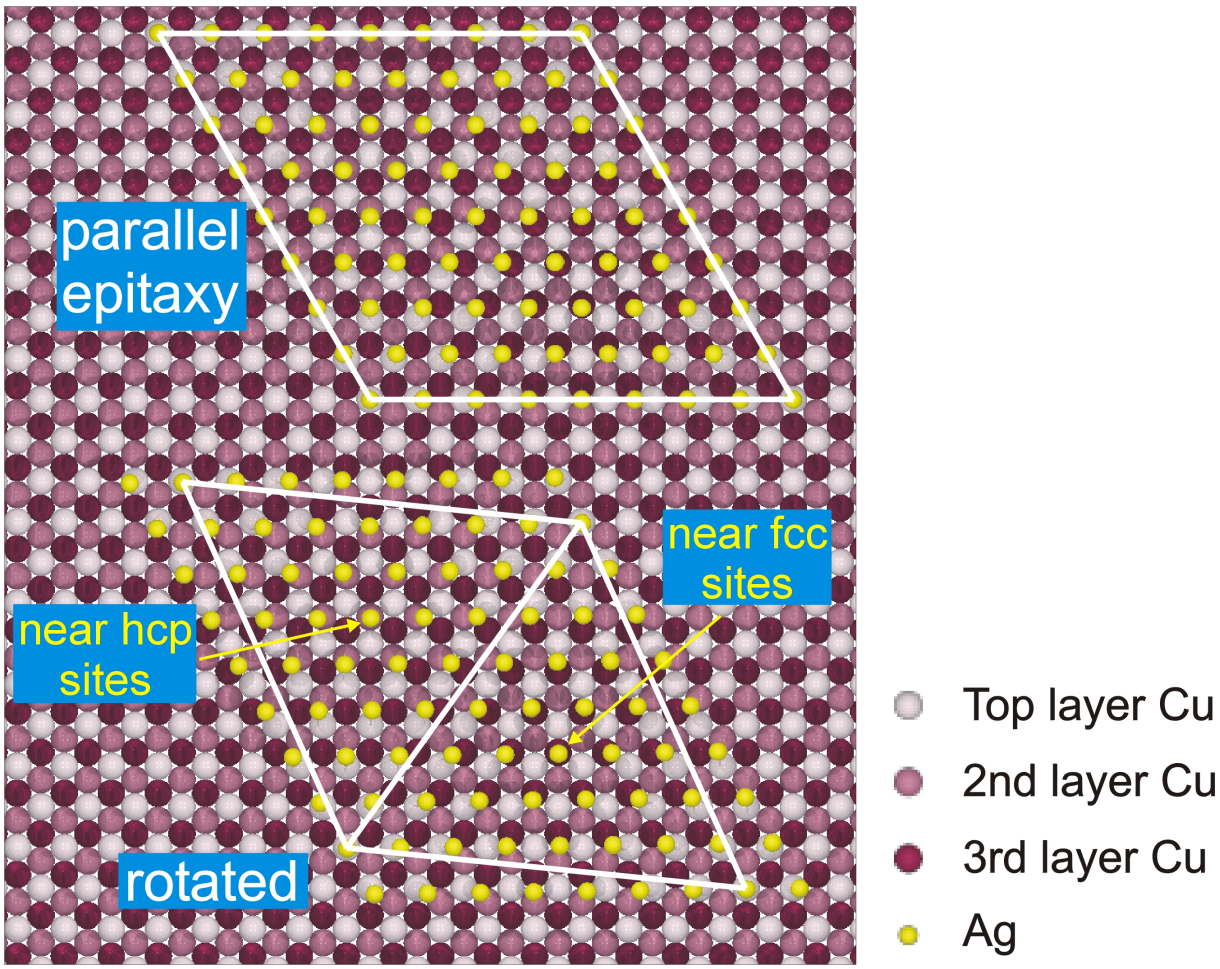

Figure 6.19: Hard-sphere model of an Ag adlayer on Cu(111) according to McMahon et al. [MHC92] the spheres represent the atomic positions, the size is arbitrary and chosen to visualize the top three layers of the Cu(111) surface
top: parallel epitaxy with a matching of Ag atoms on-top of the 1st and the 9th Cu atom causes 0.46% compressive strain in the Ag layer
bottom: counterclockwise rotation of 0.77° of the uncompressed Ag layer leads to a rhombic unit cell with two structurally inequivalent triangles; in this configuration there is virtually no lateral strain in adlayer; triangles are imaged differently with the STM (dark regions in Figure 6.18), because the Ag atoms in the center of the left triangle are close to hcp sites, whereas the one of the right triangle are close to fcc sites

close-packed rows. In the orientation of these lines there is a small angular difference of ∼1.3°. This indicates a non-parallel lattice matching of Cu(111) and Ag(111). The line scan shown in Figure 6.18b illustrates the step height of the Ag island on the Cu(111) facet. It measures ∼2.6 Å, which is close to the expected value for a monoatomic Ag(111) step of ∼2.4 Å within the uncertainty for STM height determinations.

Previous investigations of the growth behavior of Ag on a Cu(111) surface using scanning tunneling microscopy were carried out by McMahon et al. [MHC92]. The suggested overlayer configurations can be seen in the hard-sphere model of Figure 6.19. The top part shows an example where the superstructure cell is obtained for parallel epitaxy (i.e. equivalent in-plane directions in the adlayer and in the substrate are parallel) with a compressive strain of 0.46%. The 1st and the 9th Ag atom are in a coincident on-top position with respect to the Cu(111) substrate. A second configuration proposed by McMahon et al. is seen in the lower part of Figure 6.19. In this case, the Ag lattice is not compressed at all but slightly rotated counterclockwise by 0.77°. The resulting supercell is given by a rhombus which consists of two non-equivalent triangles. The difference between these triangles is the position of the Ag adatoms near the center of each triangle. These adatoms are either located near hcp (left triangle) or near fcc (right triangle) sites. In the STM images the adatoms of the hcp site would appear lower (darker), what can be clearly seen in Figure 6.18a. These facts and the slight angular difference between the close-packed rows indicate that in the present case the second structural model is valid for the Ag adsorption on the Cu(111) facet.

To summarize, Ag(111) islands can be found on the Cu(111) facet, where a coincident Ag lattice is formed by a slight rotation of 0.77°. This model is an idealization which neglects local relaxations of the Ag adlayer. In the shown STM images, the Cu(111) facet is not completely covered with Ag due to a relatively small overall Ag coverage. A higher deposition amount of Ag would lead to a complete coverage of the (111) facet.

Ag on the (311) and the (531) Facet

The (311) facet which is free of any steps for the as-grown pyramidal structure shows steps and terraces after Ag deposition (cf. Figure 6.17). Figure 6.20a shows an atomically resolved STM image of a (311) facet with a step caused by the Ag deposition. Both terraces exhibit an atomic corrugation with a square unit cell of 4 Å × 4 Å in size. A pseudomorphic Ag layer with an Ag-Ag distance of 4 Å on top of the inert NaCl adlayer is energetically unlikely. Apparently, the corrugation observed corresponds to the NaCl(100) oriented layer. That means that there is no Ag adlayer on top of the inert NaCl. As a matter of fact, the steps on the (311) facet are caused by the deposition of Ag. The terraces start to grow from the border line between

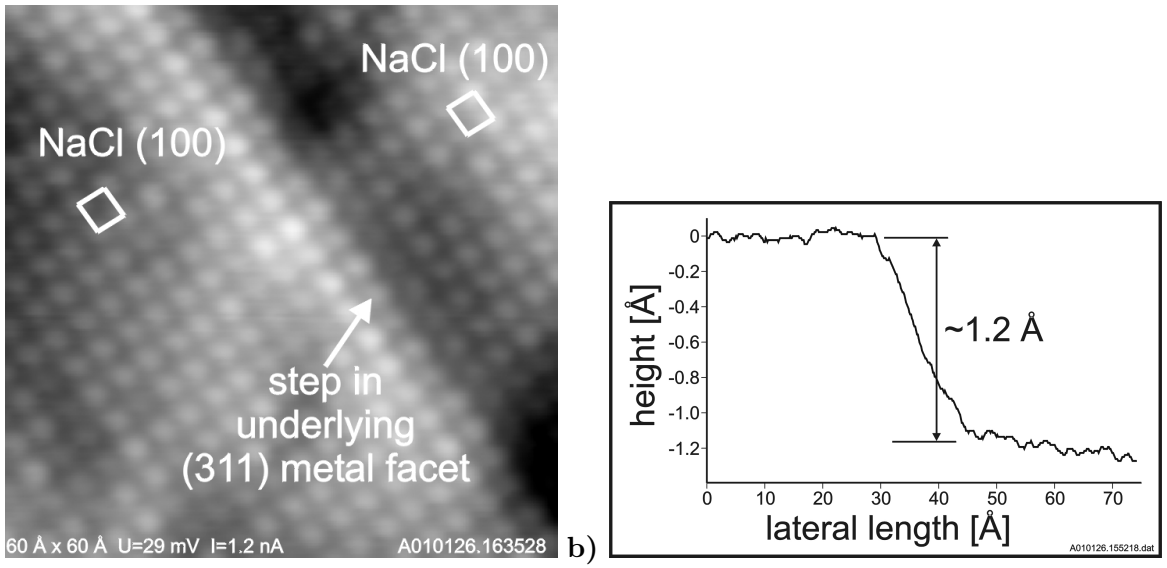

Figure 6.20: STM image and line scan of the (311) facet after Ag deposition
a) atomically resolved STM image (60 Å × 60 Å, U=29 mV, I=1.2 nA) of the (311) facet with two terraces; surface periodicity corresponds to the NaCl(100) film on both terraces
b) line scan over a step edge on the Cu(311) facet; the height of ∼ 1.2 Å is close to a monoatomic Ag(311) step (theoretical value: 1.23 Å)

this facet and the Ag-covered Cu(111) facet (cf. Figure 6.17b). These findings suggest that Ag has diffused into the interface between the NaCl film and the Cu facet. A line scan over the step edge on the (311) facet is displayed in Figure 6.20b and verifies a step height of ∼1.2 Å. This step height is close to a monoatomic step on a Ag(311) surface (theoretical value: 1.23 Å). The atomic corrugation, on the other hand, is according to that expected for bulk-terminated NaCl(100) (the STM images only the Cl ions [HRH$^+$99]). Importantly, the step causes a lateral shift of the Cl ions, which will be investigated in greater detail in conjunction with the STM image and hard-sphere models in Figure 6.21. The orientation of the Cu(311) facet is inferred from the hard-sphere model in Figure 6.7. For a better illustration, the STM image and the hard-sphere models in Figure 6.21 were rotated clockwise by ∼30° with respect to the original STM image (cf. Figure 6.20a). Hence, the intrinsic Cu steps are oriented horizontally in Figure 6.21. In the STM image, a shift of the Cl ion positions perpendicular to the intrinsic steps of the Cu template can be observed (i.e. the shift is parallel to the Ag-induced step direction). This shift is can be explained by the incorporation of a monoatomic Ag(311) layer into the interface. This layer consists of Ag atoms which are localized in the troughs of the Cu(311) template. The separation of the resulting close-packed Ag rows perpendicular to the intrinsic Cu steps is determined by the spacing of the troughs (4.23 Å). Parallel to the intrinsic steps, on the other

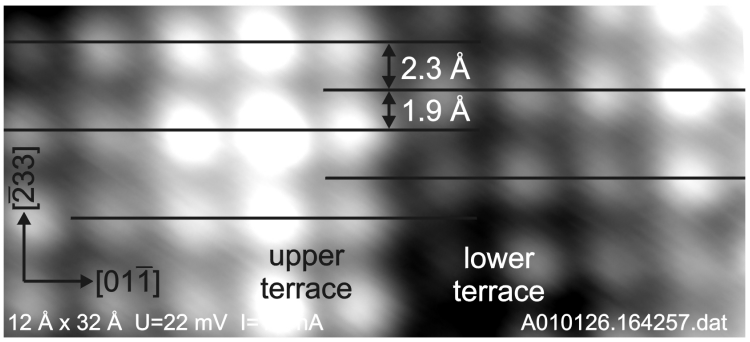

a)

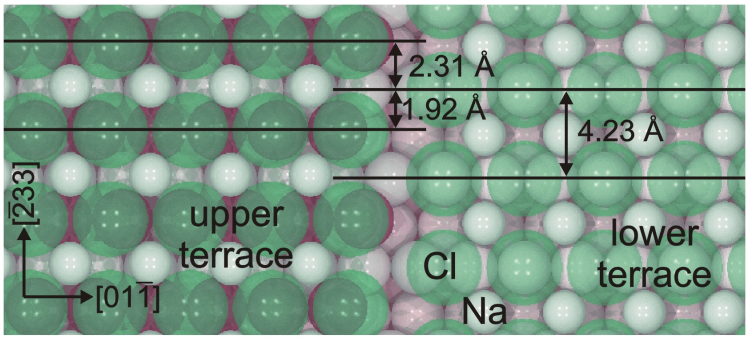

b)

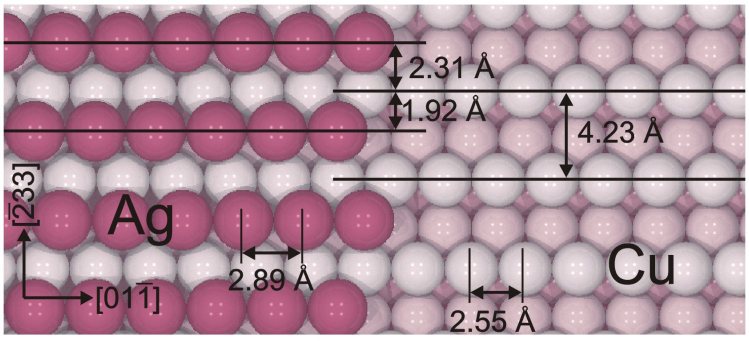

c)

Figure 6.21: STM image and hard-sphere models of the stepped (311) facet after Ag deposition
a) atomically resolved STM image (12 Å × 32 Å, U=22 mV, I=1.2 nA) of the (311) facet with two terraces; the rows of Cl ions of the upper terrace (left) which run parallel to the intrinsic steps of the (311) template are shifted by 2.3 Å in the [2̄33] direction with respect to the lower terrace (right)
b) hard-sphere model of the NaCl overlayer on the stepped (311) facet
c) hard-sphere model from b) without the NaCl adlayer; one layer of Ag atoms in (311) configuration is located on top of the Cu(311) facet (left); the result is a lateral shift of top-most close-packed metal rows of 2.31 Å in [2̄33] direction as observed for the Cl ions in the STM image above

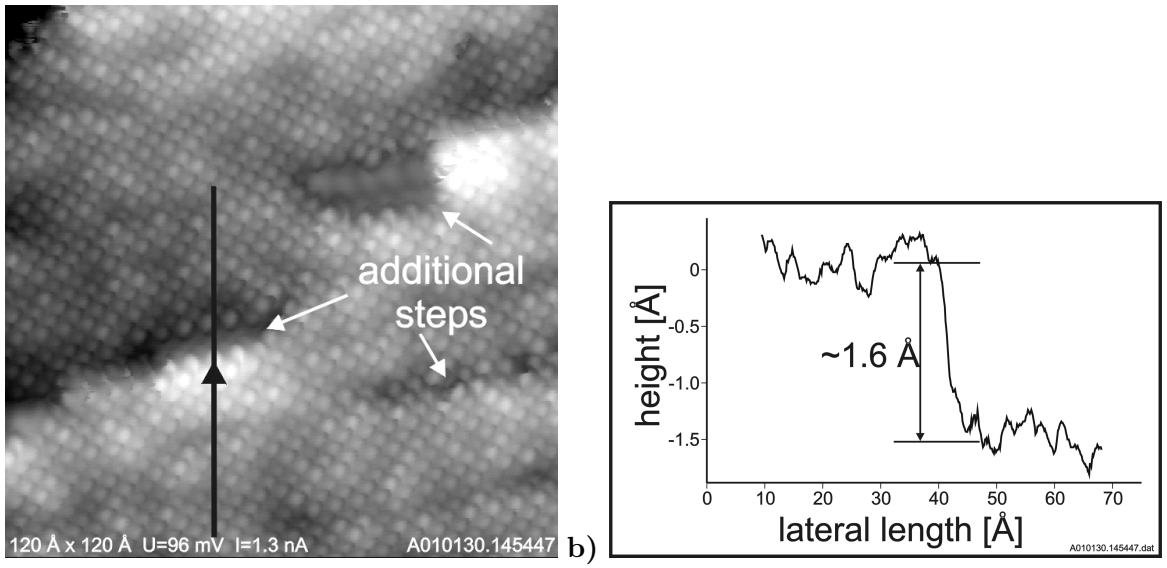

Figure 6.22: STM image and line scan of the (531) facet after Ag deposition
a) atomically resolved STM image (120 Å × 120 Å, U=96 mV, I=1.3 nA) of the (531) facet with different steps; the corrugation observed matches with NaCl(100) adlayer
b) line scan over the step edge on the facet; the step height of ∼1.6 Å is significantly different than the step height (∼0.19 Å) for the stepped (531) facet without Ag (cf. Figure 6.15b)

hand, it is likely that the close-packed Ag atom rows adopt their intrinsic Ag-Ag spacing of 2.89 Å. This situation is illustrated in the hard-sphere model in Figure 6.21c showing a bare Cu(311) terrace on the right hand side and the close-packed Ag rows located in the troughs on the left hand side. The close-packed Ag rows are shifted by 2.31 Å in the $[\bar{2}33]$ direction with respect to the top-most Cu rows on the right. Under the assumption that the Cl ions are located on top of the close-packed metal atom rows of the structure in Figure 6.21c, the configuration shown in Figure 6.21b is obtained. The Cl ions on the left hand side thus follow the lateral shift of 2.31 Å in the $[\bar{2}33]$ direction with respect to the Cl ions on the right hand side. This precisely corresponds to the experimental observation shown in the STM image in Figure 6.21a. A detailed length analysis of the Cl-Cl distances in the STM image reveals identical unit cell dimensions on both the upper terrace (left) and the lower terrace (right). This is not surprising, since the distance perpendicular to the close-packed metal rows is equal for both terraces. Parallel to the close-packed metal rows the Cl ions are free to adopt their preferred spacing. To conclude, NaCl acts as a surfactant and stabilizes the growth of a monoatomic (311)-like Ag layer on the Cu(311) facet. This growth phenomenon is observed here for the first time. In contrast to the behavior found here, Ag growth on vicinal Cu(111) surfaces is known to induce a faceting of the Cu template [BMOS01].

For the (531) facet, a similar behavior like for the (311) facet can be found. Also in this case, additional steps are incorporated after Ag deposition (see Figure 6.22a). The step height measures ∼1.6 Å (cf. Figure 6.22b), which is significantly higher than the previously described incorporation of defect steps into the Cu(531) facet for geometrical matching with the NaCl adlayer (cf. section 6.1.2). Also for this facet, the unit cell of the NaCl(100) film can be recognized, so that subsurface layer growth of Ag on the stepped (531) surface can be assumed. Due to the complicated structure of the (531) facet, the exact geometrical matching between the Ag adlayer and the Cu template could not be determined, but it can be expected that the Ag atoms are located in highly coordinated sites of the Cu(531) template, i.e. their arrangement resembles that of the kink atoms of the original Cu facet.

Conclusions for the Ag Deposition

After the deposition of Ag onto the pyramidal surface structure, Ag aggregation was found on all three facet types. Ag forms flat islands on the (111) facet with the superstructure known from previous studies [MHC92]. At sample temperatures around 300 K, there is no island growth on top of the inert NaCl layer on the other two facets. That means the faceted structures still consists of insulating (311) and (531) facets and metallic (111) facets. A very interesting and new surfactant growth mechanism was found on the two NaCl-covered facets. Ultrathin metal layers of an open structure could be stabilized by the NaCl capping layer. Ag is diffusing into the interface between the NaCl film and the Cu facets and preferably occupies highly coordinated sites, i.e. the troughs on Cu(311) and sites between kink atoms on Cu(531). To investigate this behavior in greater detail, further investigations are necessary. Due to the rather complicated structure with the different facets studied here, it is promising to choose a simpler system, like the deposition of Ag on a Cu(311) crystal which is partially overgrown by NaCl. The growth behavior for Ag at lower temperatures (∼100 K) was also investigated. The mobility and subsequently the diffusion length of Ag is reduced in this temperature regime, so that there are small islands formed on top of all three facet types. The temperature-dependent behavior of the nucleation process in competition with the interfacial diffusion process needs also to be investigated in further studies.

6.3 Summary for Two-dimensional Faceting

The enhanced interfacial stability between stepped or kinked metal surfaces and ionic insulators was exploited to fabricate a two-dimensional facet structure. The starting Cu(532) surface, which is a kinked surface, restructures after NaCl deposition into a regular assembly of nanosize pyramids whose facets show a different degree in surface chemical reactivity. Three different

facet types build up the entire facet structure: A (111) oriented Cu facet, a NaCl-covered (311) facet, and a regularly stepped Cu(531) facet, which is also overgrown by one monolayer of NaCl. This (531) facet is a kinked surface, where the NaCl adlayer induces the formation of monoatomic defect steps to achieve an optimized geometrical matching between adlayer and template. This behavior – the incorporation of defect steps to overcome strain while preserving a matching between the ionic layer and the charge modulation of the substrate – is a general observation for the systems investigated in this work.

The chemical selectivity of the nanopyramids was verified by adsorbing CO on the bare Cu(111) facet only. The deposition of Ag onto the facet structure showed a very interesting and new surfactant growth mode, where NaCl was used as a capping layer to grow an epitaxial Ag layer in an open surface structure.